

# Gamma-Ray Pulsar Revolution

Patrizia A. Caraveo

Istituto di Astrofisica Spaziale e Fisica Cosmica (IASF) - Istituto Nazionale di Astrofisica (INAF),  
20133 Milano, Italy; email: pat@iasf-milano.inaf.it

Annu. Rev. Astron. Astrophys. 2014. 52:211–50

First published online as a Review in Advance on  
June 4, 2014

The *Annual Review of Astronomy and Astrophysics* is  
online at [astro.annualreviews.org](http://astro.annualreviews.org)

This article's doi:  
[10.1146/annurev-astro-081913-035948](https://doi.org/10.1146/annurev-astro-081913-035948)

Copyright © 2014 by Annual Reviews.  
All rights reserved

## Keywords

neutron stars, gamma-ray detectors, gamma-ray sources, radio-quiet  
pulsars, millisecond pulsars

## Abstract

Isolated neutron stars (INSs) were the first sources identified in the field of high-energy gamma-ray astronomy. In the 1970s, only two sources had been identified, the Crab and Vela pulsars. However, although few in number, these objects were crucial in establishing the very concept of a gamma-ray source. Moreover, they opened up significant discovery space in both the theoretical and phenomenological fronts. The need to explain the copious gamma-ray emission of these pulsars led to breakthrough developments in understanding the structure and physics of neutron star (NS) magnetospheres. In parallel, the 20-year-long chase to understand the nature of Geminga unveiled the existence of a radio-quiet, gamma-ray-emitting INS, adding a new dimension to the INS family.

We are living through an extraordinary time of discovery. The current generation of gamma-ray detectors has vastly increased the population of known gamma-ray-emitting NSs. The 100 mark was crossed in 2011, and we are now over 150. The gamma-ray-emitting NS population exhibits roughly equal numbers of radio-loud and radio-quiet young INSs, plus an astonishing, and unexpected, group of isolated and binary millisecond pulsars (MSPs). The number of MSPs is growing so rapidly that they are on their way to becoming the most numerous members of the family of gamma-ray-emitting NSs. Even as these findings have set the stage for a revolution in our understanding of gamma-ray-emitting NSs, long-term monitoring of the gamma-ray sky has revealed evidence of flux variability in the Crab Nebula as well as in the pulsed emission from PSR J2021+4026, challenging a four-decades-old, constant-emission paradigm. Now we know that both pulsars and their nebulae can, indeed, display variable emission.

## 1. INTRODUCTION

Neutron stars (NSs) are very efficient natural particle accelerators owing to their rapidly rotating, hugely intense magnetic fields. Moreover, the accelerated particles (mostly electrons and positrons) are delivered into a highly magnetized surrounding, ideal for making them radiate high-energy gamma rays that bear the timing signature of their parent isolated neutron star (INS). In a field such as high-energy gamma-ray astronomy, which is hampered by poor angular resolution compounded by relatively low numbers of detected photons, the presence of an unambiguous timing signature has been crucial for allowing identification of gamma-ray sources with crude positions. The combination of the ideal physical conditions with the telltale time signature makes INSs the most prominent class of high-energy gamma-ray emitters in our Galaxy.

However, progress in this field has been hampered by all sorts of experimental difficulties, stemming from the paucity of gamma-ray photons. Gamma-ray pulsars cannot be detected in real time, like radio pulsars. To see pulsations, i.e., to build a statistically significant light curve, photons collected over weeks to years have to be properly phased, folding their arrival times according to precise timing parameters. Prior to doing so, however, photon arrival times must be converted to the Solar System barycenter, an ancillary yet inescapable operation upon which rests the success of the folding technique. Because such a correction is very position sensitive, precise source position is an essential bit of information for performing a search for pulsations in gamma rays. Thus, methods had to be devised to properly correct and fold the gamma-ray photon arrival times while testing the statistical significance of the results.

In the meantime, the performance of gamma-ray telescopes has improved generation after generation, going from NASA's pioneering SAS-2 (Fichtel et al. 1975) and ESA's COS-B (Bignami et al. 1975), to NASA's EGRET (Kanbach et al. 1988), to the current generation, encompassing Agenzia Spaziale Italiana's (ASI's) AGILE (Tavani et al. 2009) and NASA's *Fermi* (née GLAST, Atwood et al. 2009). Four decades of unrelenting efforts in hardware and software were needed to go from the first firm detection of a gamma-ray pulsar to a family portrait encompassing far more than 100 objects. The growth, stemming primarily from the dramatic acceleration of recent years, is impressive, as shown in **Figure 1**. In parallel, the overall quality of the data, namely the angular, spectral, and time resolution achieved for each photon as well as the overall sensitivity of the instruments, also significantly improved. This can be also seen in **Figure 1**, which shows a compilation of five sets of Vela pulsar light curves measured over a span of four decades by the five missions mentioned above.

## 2. THE PAST: WHEN SOURCES WERE FEW AND FAR BETWEEN, AND EACH ONE COUNTED

### 2.1. Pulsars as Gamma-Ray Sources

All the sky maps produced since the beginning of gamma-ray astronomy are dominated by three sources near the plane of the Galaxy. Folding the gamma photon arrival times using the radio ephemerides, SAS-2 identified first the Crab (Kniffen et al. 1974) and, later, the Vela pulsars (Thompson et al. 1975), i.e., the two brightest sources in the gamma-ray sky. The third source, shining next to the Crab in the Galactic anticenter, was named  $\gamma 195+5$  from its Galactic coordinates and could not be identified with any notable celestial object.

For the Crab, the SAS-2 detection was the confirmation of early, contradictory balloon claims (e.g., Vasseur et al. 1970, 1971), whereas for the older and less energetic Vela it was a genuine novelty. In the 1970s pulsars were astronomical newcomers, and the gamma-ray detections of Crab and Vela added an important new piece of information in the struggle to understand those extreme

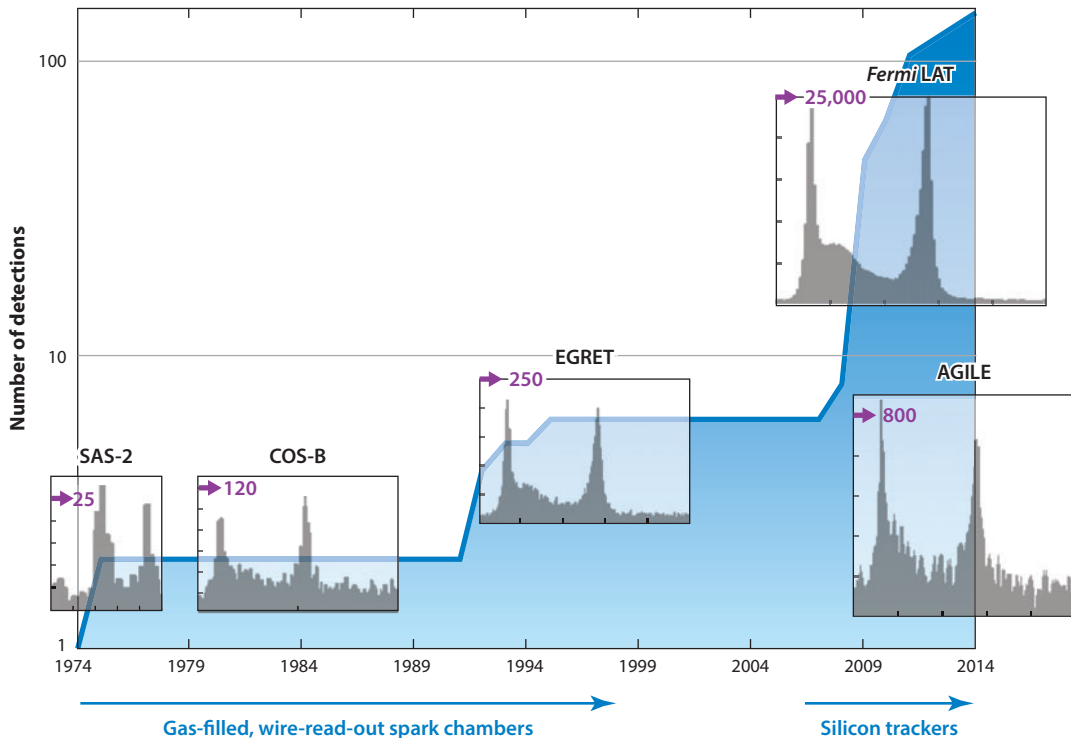


**Figure 1**

Evidence of the beneficial effects of sensitivity increase. Over four decades of gamma-ray astronomy, going from gas-and-wire to silicon detectors, the total number of gamma-ray pulsars is seen to increase by a factor of hundreds (*pale blue background area*). The phase histograms (*light curves*) of gamma-ray photons collected from the Vela pulsar by SAS-2 ( $>35$  MeV), COS-B ( $>50$  MeV), EGRET ( $>100$  MeV), AGILE ( $>100$  MeV) and *Fermi* LAT ( $>100$  MeV) are also shown. The quality and detail level obtained (i.e., number of bins that can be afforded per graph and number of photons per bin) correlate directly with the increased photon statistics, i.e., mission sensitivity. The photon counting of the highest bin in the best light curve published by each mission is shown in magenta.

stars. The seminal work by Goldreich & Julian (1969) showed that a pulsar magnetosphere, far from being a vacuum, should be filled with plasma because the induced electric force wins over the gravitational pull on surface charges. Building on this result, Sturrock (1971) laid the foundations of pulsar electrodynamics and proposed the polar cap (PC) acceleration zone. Theoretical interpretations of the SAS-2 results elaborated on this idea, with contributions from Ruderman & Sutherland (1975) and Harding et al. (1978), and were further developed by Daugherty & Harding (1982). In PC models, particles, accelerated by rotation-induced electric fields above the PC, move along the dipole magnetic ( $B$ ) field lines and produce curvature radiation. In this environment, photons above 1 GeV are absorbed by the  $B$  field and produce  $e^+ e^-$  pairs, which radiate synchrotron photons and produce a second generation of pairs. Such a cascade will continue until the synchrotron photons fail to meet the energetic requirements to pair produce and can escape to contribute to the high-energy pulsar emission. The remaining pairs may supply particles to a coherent process that is responsible for the radio emission. This process takes place at low altitudes ( $<1 R_{\text{NS}}$ , neutron star radius) above the stellar magnetic poles, where the beam of radio emission is also originating.

The premature termination of the SAS-2 mission interrupted its stream of discoveries, which was then taken up by COS-B, launched by the ESA in 1975. Similar to SAS-2 in dimensions (and,

thus, in sensitivity), COS-B lasted much longer and had ample time to confirm and significantly improve the SAS-2 findings while also discovering a population of unidentified Galactic gamma-ray sources (Swanenburg et al. 1981).

The COS-B's detailed study of Crab and Vela behavior made it clear that the measured gamma-ray emission accounted for at least  $10^{-3}$  of their rotation energy loss  $\dot{E}$  ( $\dot{E}_{\text{rot}} = -4\pi^2 IP\dot{P}^{-3}$ , where  $P$  and  $\dot{P}$  are the pulsar period and period derivative, respectively, whereas  $I$  is the moment of inertia assumed to be  $10^{45} \text{ g cm}^{-2}$ ). With a gamma-ray yield clearly dominating the pulsar emission, the gamma channel stands out as the most energetically demanding (Buccheri et al. 1978, Kanbach et al. 1980). To meet such requirements, Arons (1983) developed the slot gap (SG) model where pair creation takes place along favorably curved  $B$ -field lines above the PCs and far from the NS surface. This model works well for short period pulsars, such as Crab and Vela. Although their double-peaked gamma-ray light curves appear similar, it was then immediately clear that their ratios between the pulsar rotational energy loss  $\dot{E}$  and their gamma-ray luminosity  $L_\gamma = 4\pi d^2 F_\gamma f_\Omega$  were different (where  $d$  is the pulsar distance,  $F_\gamma$  the measured flux, and  $f_\Omega$  is the beaming factor, which depends on pulsar geometry and is assumed to be 1 steradian, i.e.,  $f_\Omega = 1/4\pi$ ). The older and less energetic Vela was more efficient than the younger and more energetic Crab. The spectral shapes of the sources were different: Although the Crab could be fitted with a single power law [ $\frac{dN}{dE} = K(\frac{E}{E_0})^{-2.1+/-0.3}$ ], for Vela a flattening at low energies combined with a steepening at high energies made a single power law fit much more challenging, if not impossible (Bennett et al. 1977). Moreover, the multiwavelength behavior of the two objects appeared vastly different. Although the Crab exhibits similar light curves at all wavelengths, Vela's light curves are radically different at different wavelengths (e.g., Bignami & Hermsen 1983). Such macroscopic effects, which could not be accounted for by the PC model, prompted Cheng et al. (1986) to propose an outer magnetosphere model, wherein particles are accelerated within the vacuum outer gap (OG) extending from the null surface (i.e., where  $\Omega \cdot B = 0$ , which spatially separates the opposing charges) to the light cylinder (a virtual cylindrical surface or radius  $R_{\text{LC}}$  where corotation stops, because  $\Omega R_{\text{LC}} = c$ ) and produce gamma rays far from the NS surface, mainly by curvature and synchrotron radiation. The OG model applies only to gamma-ray emission and disentangles the gamma-emitting region from the radio one. The PC and OG models produce gamma rays in totally different regions of the pulsar magnetosphere, relatively near the surface for the PC scenario and far away for the OG, which approaches the light cylinder. The two different locations imply different ambient  $B$  fields, and thus different emission-absorption combinations, as well as different geometry and thus different beaming. Moreover, geographically different emitting regions could come into view during the pulsar rotation, thus contributing at different pulsar phases to yield spectral shapes varying as a function of the pulsar rotation phase. The composite geometry interpretation was supported by the varying spectral shapes found in different phase intervals for the Vela pulsar by Grenier et al. (1988) in their attempt to perform phase-resolved spectroscopy.

## 2.2. More Gamma-Ray Sources: Geminga and the Rest of the Crowd

In addition to Crab and Vela, COS-B detected two dozen gamma-ray sources (Swanenburg et al. 1981) for which there were no obvious identifications. Owing to COS-B's uneven coverage of the sky, such sources were mainly located near the Galactic plane, with the notable exception of an excess positionally coincident with 3C273, the first extragalactic gamma-ray source (Bignami et al. 1981a). Particular attention was devoted to  $\gamma 195+5$ , readily dubbed Geminga (a name inspired by the gamma-ray source position within the Gemini constellation, but also a pun in Milanese dialect meaning "is not there" or "there is nothing").

Both SAS-2 (Ogelman et al. 1976) and COS-B (Buccheri et al. 1978) data were searched for pulsed signals from known radio pulsars and both claimed low significance detections. Although such results could not be confirmed, the statistical evaluation of the search outcome led to the development of the  $Z_n^2$  method of gauging the statistical significance of a light curve (Buccheri et al. 1983). de Jager et al. (1989; further elaborated by de Jager & Büsching 2010) proposed a different statistical test known as the H-test. Both  $Z_n^2$  and the H-test are now widely used.

However, no statistical test can overcome the irregularities usually present in pulsar timing behavior that hamper, and sometimes prevent, the use of archival, years-old timing information to phase-fold the meager gamma-ray photon harvest. It was quickly realized that, if the radio timing parameters are not contemporary to the gamma-ray observations, the folding must be performed over a range of  $P$  and  $\dot{P}$  values sampling the extrapolated parameter space. By multiplying the trials performed, this procedure weakens the significance of any tentative detection. Such a drawback was an important lesson learned for future instruments and pointed to the need for contemporaneous radio monitoring of promising pulsars. In the meantime, the SAS-2 and COS-B claims, though unconfirmed, spurred the discussion on the evolution of gamma-ray emission efficiency as a function of pulsar age. If true, they would have implied a steady growth of the gamma-ray yield as pulsars age. Although all those tentative detections have long been forgotten, the evolution of the gamma-ray emissivity as a function of pulsar age is still debated.

Meanwhile, by exploiting the latitude distribution of the unidentified sources (Swanenburg et al. 1981) as well as the shape of their log $N$ -log $S$  distribution (Bignami & Caraveo 1980), it was possible to compute the average source luminosity and distance, showing that young, energetic pulsars at a few-kiloparsecs distance and with efficiencies between those of the Crab and Vela could account for at least a fraction of the newly found sources. This finding spurred the search for radio pulsars within the COS-B error boxes. However, the effort took some time and its results came too late to be useful to identify COS-B sources, but it paved the way for successful identifications with the following gamma-ray mission.

In parallel, by exploiting the imaging capability of the newly launched *Einstein Observatory*, a program to cover the error boxes of several COS-B unidentified sources was successfully carried out as an alternative way to search for gamma-ray source counterparts (Caraveo 1982). Much interest was focused on Geminga (Bignami et al. 1983), by far the brightest among the unidentified sources that had already defeated radio searches, but seminal results were obtained for 2CG135+01 (Bignami et al. 1981b), for which the peculiar binary system LSI 61° 303 was proposed as a counterpart.

The chase for Geminga went on after the demise of COS-B, exploiting all the space and ground instruments available at all possible wavelengths and bridging the hiatus between COS-B and the launch of EGRET. Bignami & Caraveo (1996) have summarized the long and checkered story that led to the discovery of the first bona fide INS pulsating in X- and gamma rays but not at radio wavelengths. Indeed, the gamma-ray pulsation was found only when *Rosat* secured the X-ray periodicity detection (Halpern & Holt 1992), making it possible to fold the gamma-ray data collected almost simultaneously by EGRET (Bertsch et al. 1992) on board the *Compton Gamma Ray Observatory* (CGRO). Geminga had been pulsating all the time, of course, but the paucity of photons detected over COS-B's seven-year lifetime, together with the poor source localization, hampered the search for pulsations that could be found only a posteriori (Bignami & Caraveo 1992). In retrospect, the discovery of a radio-quiet INS should not have been totally unexpected. In view of the geometry-driven emission mechanisms believed to be at work in radio pulsars, with radio-emitting regions probably detached from the gamma-ray regions, radio-quiet objects could have been expected. However, finding the first radio-quiet INS made it clear that gamma-ray astronomy had significant discovery space of its own.

### 2.3. EGRET: More Pulsars, at Last

Apart from studying the Crab (Nolan et al. 1993), Vela (Kanbach et al. 1994), and Geminga (Mattox et al. 1992, Mayer-Hasselwander et al. 1994), EGRET, which could count on a significant contemporary pulsar radio monitoring campaign, detected three more pulsars, namely PSR B1706-44 (Thompson et al. 1992, 1996), PSR B1055-52 (Fierro et al. 1993) and PSR B1951+32 (Ramanamurthy et al. 1995), whereas PSR B1509-58 was only detected at low energy by the Comptel instrument (Kuiper et al. 1999), also on board CGRO (Gehrels et al. 1994). Exploiting Comptel data, Kuiper et al. (2001) assessed the evolution of the CRAB light curve from soft X-rays up to high-energy gamma-rays. We note that PSR B1706-44 coincides with the COS-B source 2CG342-02, but the radio pulsar was discovered after the end of the COS-B mission.

Although Nel et al. (1996), using 3.5 years of EGRET observations, computed upper limits for 350 pulsars for which radio monitoring was available, it is worth mentioning that ad hoc searches did show that three more pulsars, PSR B0656+14 (Ramanamurthy et al. 1996), PSR B1046-58 (Kaspi et al. 2000), and PSR J0218+4232 (Kuiper et al. 2000), were worthy of further investigation; however, their detections were not yet compelling. While PSR B0656+14 and PSR B1046-58 were normal radio pulsars, similar to those already detected, PSR J0218+4232 was an old recycled millisecond pulsar (MSP) characterized by extremely fast rotation coupled with a magnetic field significantly lower than that of normal pulsars. Harding et al. (2002, 2005) proposed a model for acceleration in the open field line region above the PC that seemed particularly well suited for MSPs.

Thompson (2004) provides a comprehensive review of the EGRET pulsar results. Ordering the known pulsars on the basis of their overall energy output  $\dot{E}$  divided by their distance factor ( $4\pi d^2$ ), it became immediately clear that the pulsars so far detected in gamma rays were those ranking at the top of the list, i.e., those with the most favorable combination of energetics ( $\dot{E} > 10^{34}$  erg sec<sup>-1</sup>) and distance (Thompson et al. 1999). Although this ordering does not account for important variables, such as different inclinations and viewing angles as well as different efficiencies, and its value is only as good as the (usually uncertain) distance estimate, the  $\frac{\dot{E}}{4\pi d^2}$  ranking (and its variant,  $\frac{\sqrt{\dot{E}}}{4\pi d^2}$ ) proved to be an extremely useful tool. By plotting the pulsars' gamma-ray luminosities  $L_\gamma$  as a function of the open field line voltage à la Goldreich & Julian (1969), a trend can be seen pointing to a proportionality between  $L_\gamma$  and the open field line voltage, itself proportional to  $\sqrt{\dot{E}}$  (Thompson 2004).

All pulsars exhibit a power law spectral shape with a high-energy cutoff. Light curves are usually double peaked; and the peak ratio varies with energy, with the second peak usually harder than the first (by definition, the “first” gamma-ray peak is the one that comes in phase immediately after the main radio peak). Reproducing such a double-peaked structure turns out to be an important test for pulsar models. Chiang & Romani (1992, 1994) argued that the EGRET pulsars' light curves, as well as their spectra, arise naturally from a modified version of the OG model. Working in 3D and accounting for the angle  $\zeta$  between the observer's line of sight and the NS rotation axis as well as the dipole field inclination angle  $\alpha$  (see the scheme of **Figure 2**), Romani & Yadigaroglu (1995) succeeded in reproducing the Vela light curve as measured at radio, optical, X-ray, and gamma-ray wavelengths for a very inclined geometric combination of  $\alpha = 65^\circ$  and  $\zeta = 90^\circ$ . Indeed, to produce double-peaked light curves, OG models do prefer highly inclined rotators (see also Romani 1996), whereas PC models require nearly aligned geometry, allowing magnetic inclination angles comparable to the angular extent of the PC. To overcome the PC requirements on pulsar alignment, Daugherty & Harding (1996), elaborating on the seminal work by Arons (1983) on the SG idea, extrapolated the PC acceleration region to higher altitudes, which led to a full SG model by Muslimov & Harding (2003, 2004). Here particle acceleration takes place in thin SGs along the last open field line connecting the NS surface to the light cylinder. By extending the

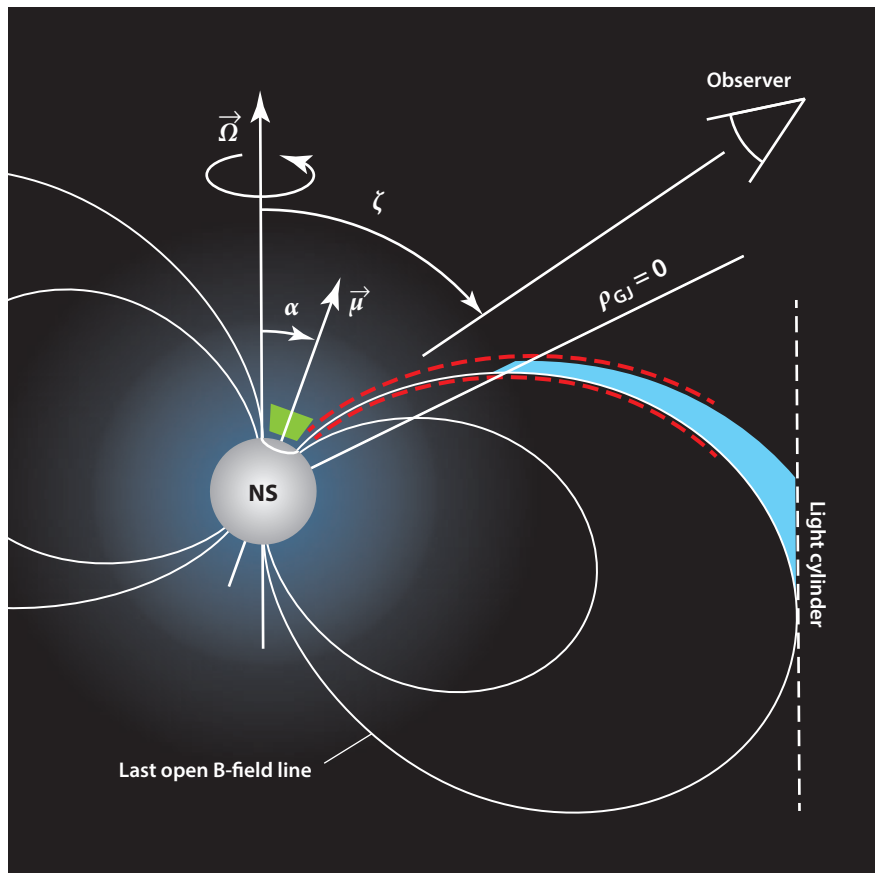


**Figure 2**

Scheme of a neutron star (NS) magnetosphere with the internal emission regions highlighted: polar cap (PC) model is in green, outer gap (OG) model in dark blue, and slot gap (SG) model in red (courtesy of J. Dyks). The striped wind scenario (outside the light cylinder) is not shown.

acceleration, and thus the gamma-ray production region, the SG can be adjusted to any magnetic inclination angle. Including special relativity effects, such as aberration and time of flight delay, in the SG framework, Dyks & Rudak (2003) developed a two-pole caustic (TPC) model that, in their opinion, can overcome some of the shortcomings of both PC and OG. To add freedom to the OG, Hirotami et al. (2003) proposed an OG that extends beyond the null surface. Production inside the light cylinder, however popular, is not the only option for pulsar modeling: Coroniti (1990) proposed a totally different approach with the striped wind model, where gamma rays are produced outside the light cylinder.

Apart from fitting light curves and spectra, models must account for the measured efficiency in converting rotational energy into gamma rays because a pulsar's gamma-ray yield is by far the dominant component of its multiwavelength emission. Romani (1996) as well as Arons (1996) discuss how to get high yields from OG and SG models. However, no model could account for a gamma-ray luminosity exceeding  $\dot{E}$ , as seemed to be the case for PSR B1055-52 (Thompson et al. 1999). That pulsar's gamma-ray luminosity, computed assuming a beaming factor of 1 steradian and using the distance derived from its radio dispersion measure (DM), required an efficiency of

more than 100%, which points to a wrong distance estimate and, possibly, too large of a beaming factor. Clearly, coupling a few percent “true” pulsar efficiency with an overestimated distance and an uncertain beaming could produce an unreasonably high gamma-ray yield.

Because the light curves of all the newly discovered EGRET pulsars appeared to be different at different wavelengths and generally not aligned in phase (see e.g., Thompson 2004), seemingly following the Vela as opposed to the Crab paradigm, the need to disentangle the radio emission region (almost certainly related to the PC) from the gamma-ray region certainly supported OG or SG emission models rather than the classical PC model.

However, though both near and far emission models could be adjusted to produce the double-peaked light curves seen by EGRET, they differed in the gamma-ray spectral shape; the PC model was unable to produce very high-energy photons. Because of the absorption in high- $B$  fields, the PC model predicts sharp, superexponential cutoffs in the observed spectra at energies of a few gigaelectronvolts. However, high-altitude models, such as OG and SG, predict a simple exponential cutoff owing to the radiation reaction limit of the accelerated particles. The EGRET sensitivity above a few gigaelectronvolts, unfortunately, did not allow discrimination between the two classes of models.

#### **2.4. EGRET: Hundreds of Gamma-Ray Sources and Many Interesting Candidates**

Although EGRET had increased the number of gamma-ray-emitting INs, pulsars were no longer the dominant celestial population in the gamma-ray sky. Extragalactic sources, many of them strongly variable, were now counted by the dozens. They greatly outnumbered the INs in the final EGRET catalog, which listed 278 sources (Hartman et al. 1999), half of which remained unidentified. However, with two-thirds of the unidentified sources clustered around the Galactic plane, pulsars, both radio-loud and radio-quiet, continued to be natural candidates to account for nonvariable sources with no obvious counterpart. Repeating the geometric exercise with the EGRET low-latitude sources, Mukherjee et al. (1995) confirmed the findings of Swanenburg et al. (1981). The unidentified low-latitude EGRET sources lay at distances between 1.2 and 6 kpc, and their luminosities range from  $0.7 \times 10^{35}$  to  $16.7 \times 10^{35}$  erg s<sup>-1</sup>, values indicating rather young and energetic INs. Gehrels et al. (2000) elaborated on the log $N$ -log $S$  distribution of the unidentified EGRET sources to claim the existence of a population of faint gamma-ray sources at mid-latitude.

Although Geminga-like INs were ideal, but elusive, potential counterparts (e.g., Yadigaroglu & Romani 1995), deep radio searches started to detect promising young and energetic pulsars within EGRET error boxes. However, finding a radio pulsar in a gamma-ray error box does not guarantee the detection of pulsations in gamma rays. As mentioned above, if the gamma-ray observations are separated in time from the radio ones, the pulsar’s period and period derivative must be extrapolated while also accounting for their uncertainties, such that the periodicity search in gamma rays must cover a vast parameter space, reducing the significance of any tentative detection. Moreover, young pulsars often exhibit timing noise and glitches that render the extrapolation much more uncertain. Thus, it should come as no surprise that the promising pulsars discovered at the end of the EGRET mission could not qualify for a solid detection of gamma-ray pulsations. As already mentioned, Kaspi et al. (2000) reported evidence of an association between the 20,000-year-old PSR B1046-58 and 3EG J1048-5840, adding this pulsar to the interesting candidates list. D’Amico et al. (2001), using Parkes data, found two young, promising radio pulsars inside the error boxes of 3EG J1420-6038 and 3EG J1837-0606. More young and energetic pulsars were found while exploring EGRET error boxes: Roberts et al. (2002) uncovered PSR J2021+3615

within the source 3EG J2021+3716 in the rich and complex Cygnus region. Yet, the pulsar timing noise prevented a meaningful back-extrapolation search for pulsations in the limited number of gamma-ray photons EGRET had collected. Similarly, PSR J2229+6114 is a young radio and X-ray pulsar whose energetics make it a plausible counterpart for 3EG 2227+6122, within which it was found, though its DM pointed to a distance value in excess of 10 kpc. If true, such a distance would have made PSR J2229+6114 too faint to be the gamma-ray source counterpart (Halpern et al. 2001b). Not surprisingly, a search for pulsations in the gamma-ray data was inconclusive. In more general terms, by cross-correlating 1,300 known radio pulsars with the EGRET catalog, Kramer et al. (2003) estimated that  $19 \pm 6$  radio pulsar associations could have been genuine.

Although the new young and energetic pulsars went onto the exploration wish list of high-energy astrophysicists waiting for the next generation of gamma-ray instruments, these examples illustrate the complex interplay between gamma-ray and radio astronomy. Indeed, the discovery of radio pulsars within gamma-ray error boxes is a story that shall recur in our narrative and grow as time goes by.

Meanwhile, a multiwavelength approach, exploiting the sequence of X-ray and optical observations that had been successfully applied to Geminga, was pursued for a number of bright, unidentified sources at medium to low Galactic latitudes. Notable examples are 3EG J1835+5918, 3EG J2020+4017, and 3EG J0010+7309. 3EG J1835+5918, a steady EGRET source with a hard spectrum and high-energy cutoff, was dubbed “Next Geminga” owing to its similarities with the prototype radio-quiet INS. *Chandra* coverage unveiled an X-ray counterpart, RX J1836.2+5925, with both thermal and nonthermal emission but without optical and radio detection, pointing, yet again, to a radio-quiet NS (Mirabal & Halpern 2001, Reimer et al. 2001, Halpern et al. 2002).

Similarly, 3EG J2020+4017 (Brazier et al. 1996) and 3EG J0010+7309 (Brazier et al. 1998) appeared to be positionally associated with the supernova remnants (SNRs)  $\gamma$  Cygni and CTA-1, respectively. The two gamma-ray sources are nonvariable and have flat spectra similar to other gamma-ray pulsars. 3EG J0010+7309 has an X-ray counterpart that, again, looks like the young INS responsible for CTA-1 embedded in its plerion (Halpern et al. 2004).

Although identified, Geminga continued to attract attention, becoming one of the most scrutinized INSs in the soft X-ray domain. Both ESA’s *XMM-Newton* and NASA’s *Chandra* X-ray observatories devoted significant observing time to this source. A long *XMM-Newton* observation unveiled a nebula trailing the NS as it moves in the interstellar medium (Caraveo et al. 2003). The same data set also allowed for phase-resolved spectroscopy to be performed, making it possible to disentangle the nonthermal, power-law component from the surface thermal emission, which was divided into hot and cool components that were seen to vary as a function of the pulsar rotational phase (Caraveo et al. 2004, de Luca et al. 2005). Using the precise knowledge of the distance to convert X-ray fluxes into luminosities, the emitting areas were computed to show that the hot component (probably linked to the PC heating by return current) comes from a surface much smaller than that of any dipole-like PC. This pointed to a quasi-aligned rotator almost perpendicular to the line of sight. The nebula detected by *XMM-Newton* was confirmed by *Chandra* (Pavlov et al. 2010), which also resolved a comet-like structure trailing the pulsar (de Luca et al. 2006).

## 2.5. The EGRET Legacy: Open Points for a New Millennium

When CGRO was deorbited in June 2000, the EGRET mission legacy in pulsar astronomy amounted to as many as ten INSs (seven firmly established detections and three probable ones). Although the objects had somewhat different phenomenology, they undoubtedly channeled the major share of their rotational energy loss into gamma rays. As shown by the energy-per-decade

plot (Thompson 2004) all the EGRET pulsar spectral energy distributions peak in the gamma-ray band. Their high efficiencies, coupled with extremely diverse multifrequency behaviors, clearly point to composite emission models, wherein different emitting regions at different locations in the pulsar magnetosphere contribute all at once. However, though the various models could account for gamma-ray emission below 1 GeV, the Rosetta stone of pulsar modeling lay in the few to 10-GeV region wherein different models predicted very different spectral shapes. Because the PC model predicts a sharp turnover at few to several gigaelectronvolts (as a result of the attenuation of the gamma-ray flux in the magnetic field above the star surface), the lack of such a turnover would rule out the already troubled PC model in favor of the OG or SG models, which produce gamma rays far from the pulsar's surface. In particular, the expected sensitivity of the Large Area Telescope (LAT), on board NASA's GLAST mission, to gigaelectronvolt photons brought hope for solving this spectral conundrum, making it possible for scientists to pin down the best emission model [as shown by Razzano et al. (2009) using simulated LAT data].

EGRET had also left a number of promising unidentified sources for which a direct search for periodicity was beyond reach, but that could be investigated at other wavelengths following the lessons learned in the chase for Geminga. Indeed, radio and X-ray searches were being actively pursued, yielding a growing number of potential gamma-ray source counterparts that were just waiting for the next gamma-ray observatories.

Expectations of pulsar detections for the coming AGILE and GLAST missions were rather uncertain, mainly due to considerable uncertainty as to which pulsar model to use. Back-extrapolating the  $\log N$ - $\log S$  number-flux relation of the EGRET pulsars, Thompson (2004) predicted a grand total ranging from 30 to 100 GLAST detections, considering both radio-quiet and radio-loud INs. On the basis of Monte Carlo simulations for PC-emitting pulsars, Harding et al. (2002) predicted the gamma-ray detection of 90 radio-loud and 101 radio-quiet pulsars. However, less than 10% of the radio-quiet pulsars were expected to yield a pulsed signal with the techniques available at the time. Simulations including OG emission models (Harding et al. 2007) yielded a large number of radio-quiet gamma-ray pulsars coupled to a comparatively small number of radio-loud ones, making it clear that the ratio of radio-quiet to radio-loud pulsars detected by GLAST would provide a useful clue in discriminating between the two classes of models. Moreover, Harding et al. (2005), on the basis of their PC model, predicted that several MSPs could be detectable by AGILE and GLAST, both yet to be launched.

Building on the lessons learned during past missions, careful campaigns involving all the major radio observatories were orchestrated to maximize the chances of success for detection of radio pulsars. Smith et al. (2008) describe the observing campaign organized by the GLAST collaboration together with all the major radio observatories (now known as the Pulsar Timing Consortium) to monitor about 200 pulsars selected for their large spin-down power ( $\dot{E} > 10^{34}$  erg sec<sup>-1</sup>) and ranked high according to their  $\frac{\sqrt{\dot{E}}}{4\pi d^2}$ . This effort also included careful calibration of the spacecraft clock (Smith & Thompson 2009, Abdo et al. 2009a) to allow for precise phase alignment of the radio and gamma-ray light curves. This rendered possible phase-folding of MSPs, a class of NSs often in binary systems, certainly interesting but not considered a prime target for the mission, in view of their rather low surface  $B$  field. For the radio-quiet Geminga, Jackson & Halpern (2005) undertook the task of maintaining phase-coherent timing parameters through biannual *XMM-Newton* measurements.

Preparation efforts were also carried out in the software domain. Extensive "data challenges," relying on massive Monte Carlo simulations (Baldini et al. 2006) of the gamma-ray sky, were conducted within the GLAST collaboration to test and debug the analysis software, with the goal of having a fully functional analysis pipeline ready at the time of launch.

Meanwhile, to meet the challenge of detecting pulsations using only the gamma-ray photons, Atwood et al. (2006) devised a new strategy to optimize the computing power needed to perform comprehensive blind searches covering a wide range of  $P$  and  $\dot{P}$ . Because very long exposure times, which are mandatory in gamma-ray astronomy, make complete Fourier analysis computationally prohibitive, the newly proposed method analyzes the differences of photon arrival times (up to a window of the order of weeks) rather than the time series itself and succeeds in maintaining good sensitivity while greatly reducing the effects of frequency derivatives and glitches. The time-difference method was successfully tried on EGRET data (Ziegler et al. 2008) and was ready to be tested on new gamma-ray data.

### 3. THE PRESENT: THE SILICON ERA IN GAMMA-RAY ASTRONOMY

The current new era in gamma-ray astronomy is characterized by significant hardware improvement owing to the introduction of the silicon-strip detector as the core constituent of a “solid-state” spark chamber (as opposed to the gas-filled, wire-read-out spark-chambers on board SAS-2, COS-B and EGRET) used to detect and track photons and to discriminate between them and the much more numerous charged particles. Silicon trackers are self-triggering devices that reduce the dead time to almost zero, enhancing the instrument’s timing and count-rate capabilities while also improving its spectral and spatial resolution. Moreover, their very compact structure allows for the design of gamma-ray detectors with steradian-sized fields of view (FoVs), thus increasing the effective observing time for any given direction in the sky. In recent years, we have been living in an ideal time for high-energy astrophysics with two such instruments operating in orbit allowing, for the first time since the beginning of gamma-ray astronomy, almost continuous coverage of the sky, with the added possibility for each to independently prove (or disprove) the other’s claims.

The two satellites are AGILE (Tavani et al. 2009), a small Italian mission of the Italian Space Agency (ASI) in close collaboration with the Istituto Nazionale di Astrofisica (INAF) and the Istituto Nazionale di Fisica Nucleare (INFN), and *Fermi* (the name given to GLAST in orbit; Atwood et al. 2009), a much bigger NASA mission with important international participation from Japan, France, Italy (again with ASI, INAF, and INFN) and Sweden.

#### 3.1. April 2007: Enter AGILE

AGILE features a silicon tracker made of 12  $40 \times 40$  cm trays and a thin calorimeter. The mass of the calorimeter is a limitation for the detection of photons with energies greater than tens of giga-electronvolts, but AGILE excels at low energies ( $E < 100$  MeV). Above the tracker, another layer of silicon acts as a hard X-ray detector and is known as SuperAGILE. Although the dimensions of AGILE are about a quarter of those of EGRET, the effective areas of the two instruments are comparable thanks to the superior performance of the silicon tracker and analog read-out, with AGILE enjoying significantly better angular and time resolution, as well as a much smaller dead time.

Launched in April 2007 from the Indian base of Sriharikota, AGILE was put into a nearly equatorial orbit and started its observing program as a pointing mission characterized by a very large FoV, covering one-sixth of the sky. As usual, AGILE carried out its “on-orbit” calibration using the Vela and Crab pulsars as targets and tested its capabilities on Geminga and PSR B1706-44 (Pellizzoni et al. 2009a). After subtracting the pulsed photons from the Vela source, a faint diffuse emission appeared, yielding the first clear detection of a resolved pulsar wind nebula in high-energy gamma rays (Pellizzoni et al. 2010).

The first new gamma-ray pulsar was discovered as part of the AGILE Guest Observer Program by Halpern et al. (2008), who detected gamma-ray emission from PSR J2021+3651 showing that

its radio distance was indeed overestimated. Thus, PSR J2021+3651 entered the stage as one of the contributors of the notoriously complex Cygnus region. Next Geminga was also closely scrutinized to ascertain its spectral shape as well as search for possible variability (Bulgarelli et al. 2008).

Folding the gamma-ray photon arrival times using contemporary ephemerides for the 35 top-ranking radio pulsars (for which radio monitoring had been organized), AGILE detected three new pulsars (Pellizzoni et al. 2009b), namely PSR J2229+6114, discovered by Halpern et al. (2001a) within the 3EG 2227+6122 error box; PSR B1509-58, a very energetic pulsar that had been seen by COMPTEL but not by EGRET owing to its very soft spectrum; and PSR J1824-2452, an MSP detected clearly for only a fraction of the observing time. PSR B1509-58 was further investigated by Pilia et al. (2010). Moreover, Pellizzoni et al. (2009b) found tantalizing signals for four more objects, namely PSRs J1016-5857, J1357-6429, J2043+2740, and J1524-5625. Of these, only the latter, which was also the least significant, was not independently detected by *Fermi*. By doubling the EGRET pulsar harvest, including the detections of the second youngest as well as the million-year-old PSR J2043+2740, AGILE was showing that gamma-ray emission is a common feature of high-ranking radio-loud pulsars, be they young or old.

### 3.2. June 2008: Enter *Fermi* and the Discovery of a New Geminga

In June 2008 GLAST was launched, and thus the *Fermi* observatory was born featuring two major instruments: the LAT (Atwood et al. 2009) and the Gamma Burst Monitor (GBM; Meegan et al. 2009). The LAT's modular structure, containing 16 towers, each featuring an 18-tray tracker sitting on a heavy calorimeter, makes it the most powerful gamma-ray telescope ever. Very well suited to detecting photons in the gigaelectronvolt range, where angular resolution is at its best, *Fermi* aimed at obtaining the sharpest (and deepest) vision of the gamma-ray sky. With a FoV of 2.4 steradian, *Fermi* was designed to primarily operate in scanning mode, covering the whole sky every three hours, i.e., once every two 90 min. orbits. Such an operating mode provides reasonably homogeneous sky coverage and guarantees that any given point in the sky is within the instrument FoV for approximately one-sixth of the time. Once in orbit, *Fermi* executed a planned calibration sequence of pointed observations during which the satellite pointed first at the Vela pulsar and, when the target was occulted by the Earth, at the EGRET unidentified source 3EG J0010+7309, coincident with the CTA-1 SNR.

Thanks to the instrument performance, the software readiness, the differencing technique, and the availability of a precise X-ray position, *Fermi*'s on-orbit verification phase yielded the long-sought detection of periodicity from 3EG J0010+7309, making it the first high-visibility result (Abdo et al. 2008) from the new *Fermi* observatory. While 3EG J0010+7309 was quite a robust INS candidate, with a faint X-ray source surrounded by diffuse emission pointing to an NS embedded in a pulsar wind nebula (Halpern et al. 2004), the speed of the discovery was amazing, boding well for the future capability of *Fermi* as a hunter of radio-quiet pulsars (Bignami 2008).

The pulsar timing parameters yielded a characteristic age ( $\tau_c = \frac{P}{2\dot{P}}$ ) of 14,000 years (comparable to the CTA-1 SNR age) and a rotational energy loss of  $4.5 \times 10^{35}$  erg s<sup>-1</sup>, i.e., a radio-quiet INS 50 times younger and 10 times more energetic than Geminga. Its dipole *B* field is rather high ( $1.1 \times 10^{13}$  G), which makes PRS J0007+7303 the second-highest magnetic field pulsar after PSR B1509-58. However, unlike PSR B1509-58, the newly discovered INS does emit high-energy photons. The pulsar light curve displays a double-peaked structure similar to that of PSR B1706-44, one of the historical EGRET pulsars that has a similar age. For radio-quiet pulsars, distance estimates rely on indirect methods such as X-ray line-of-sight absorption or their association with an SNR. Combining the radio and X-ray pieces of information, the best distance to PSR J0007+7303 is  $1.4 \pm 0.3$  kpc (Pineault et al. 1993). This makes it possible to compute the pulsar luminosity—and

thus its efficiency—that turns out to be about 1%. Interestingly, the efficiency of PSR J0007+7303 in converting its rotational energy loss into gamma rays is similar to that of PSR B1706-44, but smaller than that of the much older Geminga. Although PSR J0007+7303 is a Geminga-like gamma-ray pulsar with an X-ray counterpart, we note that, unlike Geminga, the gamma rays were the driver behind the periodicity discovery. The source faintness in X-rays prevented the detection of pulsations in that band. Only a long *XMM-Newton* observation, coupled with the precise knowledge of the gamma-ray timing parameters, yielded the X-ray pulsation detection (Caraveo et al. 2010). The X-ray counterpart of PSR J0007+7303 is a faint source, excellent for getting an accurate position, but of hardly any use for unveiling a hidden periodicity.

Pulsations from the radio pulsar PSR J1028-5819, freshly discovered by Keith et al. (2008) within 3EG J1027-5817, followed quickly (Abdo et al. 2009h), identifying the pulsar as being responsible for at least part of the flux of 3EG J1027-5817. Next came the detection of gamma-ray pulsations from PSR J0205+6449 in 3C58, a Crab-like 800-year-old SNR (Abdo et al. 2009b). The pulsar light curve is also Crab-like, and its two peaks are aligned with the X-ray ones (but not with the single radio pulse).

An impressive light curve of the Vela pulsar, including 32,400 pulsed photons collected during the verification phase, was quickly published (Abdo et al. 2009i) with a revealing spectral study of the phase-averaged gamma-ray emission. The shape of the light curve as a function of energy confirms the dramatic energy evolution hinted at by previous experiments with the appearance of a third peak in the bridge region above 1 GeV and the disappearance of the first peak at energies above 10 GeV. The *Fermi* spectrum can be described as a power law with exponential cutoff  $\frac{dN}{dE} = K \left(\frac{E}{E_0}\right)^{-\Gamma} \exp\left(-\frac{E}{E_{\text{cut}}}\right)^b$ , spectral index  $\Gamma = 1.5$ , an energy cutoff  $E_{\text{cut}} = 2.9$  GeV, and a  $b$  of  $0.88 \pm 0.4$ . This rules out any superexponential absorption that would have been the signature of attenuation owing to the interaction of high-energy gamma-ray photons with the strong magnetic field at low altitude in the pulsar magnetosphere. Thus, the lack of hyperexponential absorption points to high-latitude emission. This finding is strengthened by the detection of pulsed photons up to 17 GeV, an emission that must arise at  $R > 3.8 R_{\text{NS}}$  (from Baring 2004).

The first high-quality *Fermi* pulsar spectrum set the stage for gamma-ray emission far from the NS surface in the outer magnetosphere, near the light cylinder, ruling out the PC model in favor of the OG or SG models.

### 3.3. Surprises: Expected and Unexpected

Whereas gamma-ray emission from young, energetic pulsars (both radio-loud and radio-quiet) was widely expected, the detection of the MSP PSR J0030+0451 (Abdo et al. 2009j) came as a real surprise, mainly because such old, recycled pulsars were not supposed to be ideal gamma-ray emitters given that their surface  $B$  fields are  $10^4$  times weaker than those of young NSs. Conversely, the pulsar gamma-ray phenomenology was pretty normal looking: two narrow peaks, separated by 0.44 in phase, a spectrum well described by a power law with an exponential cutoff. However, its rather low rotational energy loss of  $3.5 \times 10^{33}$  erg  $\text{s}^{-1}$ , coupled with the parallactic distance of 300 pc and the measured flux ( $E > 100$  MeV) of approximately  $7 \times 10^{-8}$   $\text{cm}^2 \text{sec}^{-1}$ , implied a huge 15% gamma-ray production efficiency.

The detection of PSR J0030+0451 opened the way for a systematic search for gamma-ray emission from MSPs. Owing to the radio monitoring campaign (Smith et al. 2008), MSPs with  $\dot{E}$  above  $10^{34}$  erg  $\text{sec}^{-1}$  had contemporary ephemerides to be used for phase folding. The search immediately yielded interesting results; 7 more MSPs were found in a matter of months (Abdo et al. 2009c). Although MSPs are often in binary systems, we continue to refer to gamma-ray pulsars as INs, because their emission is powered only by their rotational energy loss. With

gamma-ray light curves and spectra similar to those of young pulsars, the emission regions for MSPs should also have been far from the NS surface. Although young pulsars and MSPs have vastly different B-fields at the stellar surface, the value of the  $B$  field at the light cylinder is similar, indicating a region where similar conditions naturally occur.

All the eight gamma-ray emitting MSPs were field objects, both isolated and in binary systems. The detection of the globular cluster 47 Tuc (Abdo et al. 2009d) was therefore attributed to the integrated emission of multiple MSPs within it. The case of 47 Tuc is not unique; *Fermi* has detected a dozen more globular clusters as point sources (Abdo et al. 2010a, Kong et al. 2010). In parallel, blind searches over a five-month observing interval yielded 15 more radio-quiet INs, making it clear that radio-loud and radio-quiet sources were evenly contributing to the *Fermi* pulsar harvest. Abdo et al. (2009e) discuss the general properties of the population of 16 radio-quiet INs discovered by *Fermi*. Because 13 of them were found within formerly unidentified EGRET sources that were among the set of suspected pulsars, deep X-ray investigations were already available. Indeed, 6 of the 16 pulsars were discovered by assuming a counterpart position derived from previous X-ray coverage or from newly obtained observations, using mainly the Swift X-ray Telescope. Apart from CTA-1, the newly discovered gamma-ray pulsars featured Next Geminga (Halpern et al. 2004), Gamma Cyg (Brazier et al. 1996), the Rabbit (Ng et al. 2005), Taz (Roberts & Brogan 2008), and the Eel (Roberts et al. 2001). However, the faintness of the X-ray counterparts made it clear that, for gamma-ray pulsars, the LAT's potential as a pulsation discoverer was vastly superior to that of X-ray telescopes.

The timing parameters of the 16 gamma-ray-selected pulsars point to rather young INs, with energetics similar to that of radio-loud ones. Also, their averaged fluxes, light-curves, and spectra were no different than that of radio-loud pulsars. Subsequent deep radio observations yielded detections for three of the new pulsars—two rather normal looking and one exceedingly faint (Camilo et al. 2009, Abdo et al. 2010h).

A closer look at bright sources such as Vela (Abdo et al. 2010e), Crab (Abdo et al. 2010c), and Geminga (Abdo et al. 2010f), as well as Next Geminga (Abdo et al. 2010d), for which phase-resolved analysis was possible, clearly revealed that both spectral index and cutoff energy vary as a function of the pulsar phase, confirming early findings and adding a wealth of fine structure details. The detection of the Crab pulsar at  $E > 100$  GeV by Magic and Veritas (Aliu et al. 2008, 2011; Aleksic et al. 2012) is well above any reasonable extrapolation of the *Fermi* LAT best spectral fit, pointing to a different emission mechanism for that high-energy component.

The first *Fermi* catalog of gamma-ray pulsars (IPC) lists 46 high-confidence pulsars detected within the first 6 months of the mission (Abdo et al. 2010b). Out of 46 NSs, 29 were detected in radio (further divided between 8 MSPs and 21 young pulsars) and 17 seen only in gamma rays (i.e., 16 discovered by LAT + Geminga). As expected, a significant fraction of the newly discovered LAT pulsars were found within the error boxes of high-interest EGRET unidentified sources. IPC contains 15 such cases, 13 of which are radio-quiet and 2 radio-loud, namely PSR J1028-5918 (Abdo et al. 2009h) and PSR J2021+3651 (Abdo et al. 2009f).

A power law with an exponential cutoff can fit the spectra of all 46 gamma-ray pulsars. Their light curves are usually double peaked (with peak separation of 0.4–0.6), but a nonnegligible minority of single-peaked pulsars is also present. With very few exceptions, the gamma-ray peaks are not aligned with the radio ones, confirming early EGRET findings and pointing to an emission region far from the pulsar's surface.

To assess the luminosity of gamma-ray pulsars ( $L_\gamma = 4\pi d^2 F_\gamma f_\Omega$ ),  $f_\Omega = 1$  was used for all pulsars. It is a big change compared with the past, when this parameter was assumed to be  $1/4\pi$ , and is a direct consequence of the new preference for the OG model (see, e.g., Watters et al. 2009). The gamma-ray light curves and spectral shapes point to high-altitude emission regions

producing fan beams that cover a large fraction of the celestial sphere. However, when computing the luminosity of LAT pulsars, the major source of uncertainty remains the assumed distance, because few INSs have a measured parallax. Although the majority of radio pulsars can rely on DM, distances for radio-quiet pulsars can be obtained only from X-ray absorption data, when it is available. This limits the number of radio-quiet pulsars in the *Fermi* luminosity plot.

Abdo et al. (2010b) show that the evolution of the gamma-ray luminosity as a function of the pulsar rotational energy loss cannot be fitted by a single function. Even considering the distance uncertainties, a substantial scatter is present, possibly arguing against the assumption of a common beaming factor for all objects. MSPs seem to climb more steeply in luminosity than the young pulsars, which evolve more gently.

### 3.4. *Fermi*'s Treasure Hunt

Numerous multiwavelength studies were triggered by the first wave of *Fermi* results, directly linked to both pulsars and, more generally, newly detected sources with no identification, first in the Fermi Bright Source Catalog (often referred to as 0FGL; Abdo et al. 2009g), and later in the First List of *Fermi* Sources, known as 1FGL (Abdo et al. 2010g). On the high-energy side, both exploratory and in-depth X-ray observations were carried out targeting the newly discovered radio-quiet INSs as well as the promising candidates that were emerging from the *Fermi* data, but that needed better position information to secure a statistically significant pulsation detection. On the low-energy side, the time-honored exercise of searching for radio pulsars within unidentified source error boxes was started anew. By exploiting the smaller *Fermi* error boxes, as well as more powerful analysis systems, it was possible to significantly reduce the time needed to cover each source. This allowed for multiple visits, a strategy that proved crucial to detecting radio emission from MSPs in binary systems. To maximize the chances of success, sources to be studied were selected on the basis of their “pulsariness,” a parameter quantifying the lack of variability coupled to a suitably curved spectral shape (Ackermann et al. 2012a).

Having searched 25 such pulsar-like unidentified sources, Ransom et al. (2011) reported the detection of 3 new MSPs. Such a high success rate triggered the chase for field MSPs in unidentified pulsar-like *Fermi* sources, preferably at medium to high Galactic latitude. Keith et al. (2011) found 2 MSPs and a young pulsar in their coverage of 11 *Fermi* sources. Cognard et al. (2011) unveiled two MSPs, whereas Kerr et al. (2012) found 5 MSPs after having searched 14 unidentified *Fermi* sources. Once the timing parameters of the often-binary new MSPs were accurate enough, they were also detected in gamma rays, increasing the share of this class of rather faint gamma-ray emitters (both isolated and in binary systems). More searches focusing on the unidentified sources with high pulsariness listed in the second *Fermi* source catalog (hereafter referred to as 2FGL; Nolan et al. 2012) are being conducted, and the rate of discovery is impressive, as shown in **Figure 3**.

Although this is a major result on its own (because it increases significantly the number of known field MSPs; e.g. Caraveo 2010), the sudden jump in the MSP number revived the interest of the radio-astronomical community in using these super stable clocks to detect nanoHertz gravitational waves (GWs). The slight variations GWs may induce in the time of arrival of signals coming from widely separated pulsars will be correlated, thus allowing for the direct detection of GWs (e.g., Jenet et al. 2005). Recent re-evaluation (Cordes & Shannon 2012) of the method sensitivity shows that 5 years of monitoring of (at least) 20 carefully selected MSPs stands a fair chance of detecting the GW background, allowing us to study its spectrum. Of course, a higher number of MSPs, ranging from 50 to 100 objects, would provide firmer results. Indeed, by finding so many new MSPs, *Fermi* increases the number of targets to be monitored, searching for GW induced variations. The high success rate of *Fermi*'s treasure hunt also implies that MSPs could

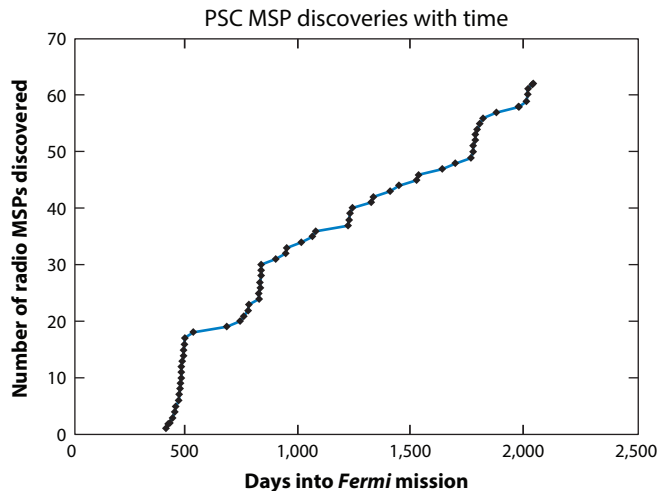


**Figure 3**

Cumulative view of the millisecond pulsars (MSPs) discovered in radio by the Pulsar Search Consortium (PSC), observing promising unidentified *Fermi* sources. Since the potential for discovery of such a technique was realized, the MSP discoveries have been continuous and no flattening in the growth curve is in sight. (Courtesy of Elizabeth Ferrara.)

play a major role in accounting for unidentified Galactic gamma-ray sources, especially the faint, high-Galactic latitude sources.

Normal young pulsars, however, should not be totally forgotten. Camilo et al. (2012), for instance, during the radio coverage of 1FGL J2030.0+3641, found a middle-aged radio pulsar that was also immediately detected in gamma rays. Indeed, as stated by Camilo et al. (2012), the fact that so few young isolated pulsars have been found in LAT sources (which are mostly along the plane) is a testament to how good the radio surveys were.

Meanwhile, blind searches were conducted in newly discovered, low-latitude pulsar-like LAT sources, selected on the basis of their pulsariness. Eight radio-quiet INSs were rapidly found (Saz Parkinson et al. 2010), and two more were added later (Saz Parkinson et al. 2011).

Although optimized through the time-differencing techniques, blind searches on ever fainter LAT sources had to cover progressively longer time spans, becoming very computer intensive and thus hampering the *Fermi* LAT's potential for discovery. To overcome the limitation in computing power, the Albert Einstein Institute in Hannover brought their supercomputer (mainly devoted to the search for GWs) into play, coupled with a new hierarchical search method originally aimed at detecting continuous GWs from rapidly rotating NSs. The reward was immediate. Nine INSs were quickly found (Pletsch et al. 2012a). PSR J1838-0537 was added later (Pletsch et al. 2012b), and its timing analysis shows that in September 2009 the pulsar suffered the largest glitch seen so far in any gamma-ray-only pulsar. Also, standard analysis using radio pulsar timing parameters continued, relentlessly following each potentially interesting pulsar because, if a pulsed signal is present, its significance grows with time and eventually reaches the 5-sigma level needed to announce a detection.

In view of the results obtained, the selection criteria used to build the list of pulsars under radio monitoring were revised, lowering the threshold  $\dot{E}$  with a proportional increase in the number of pulsars under continuous investigation. A lot of work was also devoted to improving the gamma-ray analysis technique. A weighting algorithm was introduced to assign to each photon

a weight according to its (energy-dependent) probability to come from a given pulsar (Kerr 2011). Such a weighting algorithm reduces the trials previously needed to optimize the extraction region together with the energy range and results in an enhanced sensitivity to the pulsation detection.

In parallel, Ray et al. (2011) improved the analysis techniques by applying a maximum likelihood method to extract pulse times of arrival from unbinned photon data. Using new phase-connected pulse timing solutions for the first group of 16 gamma-ray-selected pulsars, they were able to improve the source positioning, rivaling the X-ray in localization accuracy. Moreover, continuous folding unveiled the presence of glitches for PSRs J0007+7303, J1124-5916, and J1813-1246 (Ray et al. 2011), joining several other radio pulsars for which gamma-ray folding had already highlighted glitches and starting with the very first detection of a glitch from PSR B1706-44 in just 10 weeks of data (Saz Parkinson 2009). Indeed, it turns out that continuous gamma-ray coverage, coupled with the sensitivity of folding to pulsar parameters, is a powerful way to unveil pulsar glitches.

#### 4. TOWARD THE *FERMI* GAMMA-RAY PULSAR REVOLUTION

After so many advancements, it was time to publish a second pulsar catalog on the basis of three years of *Fermi* data. The number of pulsars detected was already beyond the most optimistic guesses published prior to launch. Although Thompson (2001) bracketed the expectations between 30 and 100 objects, when the *Fermi* three-year observation database was frozen, 117 pulsars met the 5-sigma pulsation significance threshold (hereafter 2PC; Abdo et al. 2013). **Figure 4** shows the

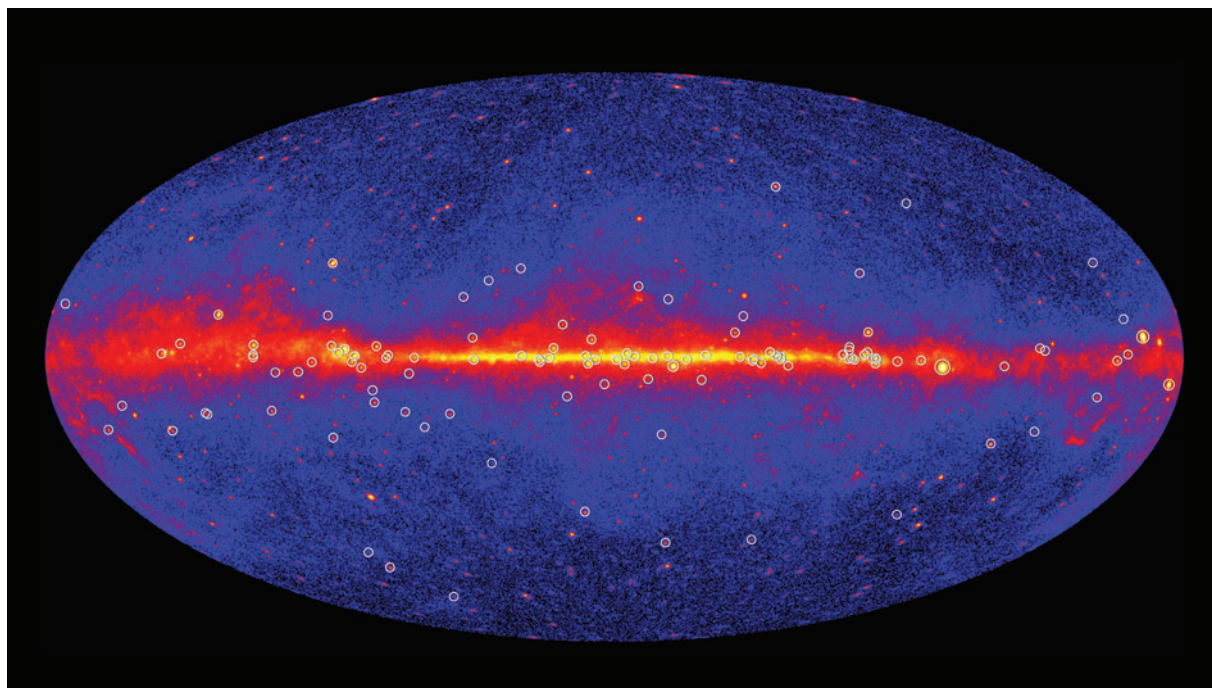


**Figure 4**

*Fermi* five-year sky map showing the positions of the 117 pulsars listed in the 2PC (Abdo et al. 2013). Image from NASA/DOE/*Fermi* LAT Collaboration (<http://svs.gsfc.nasa.gov/vis/a010000/a011300/a011342/>).

pulsar positions against the 5-year *Fermi* image of the gamma-ray sky. Of these, 42 are radio-loud pulsars and 35 are radio-quiet; 40 are MSPs, 20 of which were found through radio searches within unassociated *Fermi* LAT sources. Indeed, by the time the catalog was ready for publication, the number of MSPs discovered within unidentified sources had grown to 46 (Ray et al. 2012), 34 of which have been seen to pulsate in gamma rays.

Regarding the radio-quiet pulsars, a little clarification is in order. Out of the 36 INs discovered by *Fermi* through blind searches, two (PSR J1741-2054 and PSR J2032+4127) were subsequently detected in radio (Camilo et al. 2009) and are thus counted as radio pulsars. By contrast, PSR J1907+0602 (Abdo et al. 2010h) and PSR J0106+4855 (Pletsch et al. 2012a), both of which have been detected with exceedingly low radio fluxes, remain in the radio-quiet (or radio-faint) class. This class contains 34 *Fermi* pulsars to which Geminga (as a prototype example of a truly radio-quiet pulsar) should be added.

The 2PC (Abdo et al. 2013) represents a milestone in pulsar astronomy. First of all, it establishes *Fermi* LAT as a powerful pulsar discoverer. Indeed, half of the pulsars listed in the 2PC (Abdo et al. 2013) were not known prior to the launch of *Fermi*, and they have been either discovered by *Fermi* through blind searches or, thanks to *Fermi*, by radio targeted searches of *Fermi* LAT unassociated sources. Moreover, the 117 entries are divided almost exactly *in partes tres* between young radio-loud pulsars, young radio-quiet pulsars, and MSPs. Indeed, the most dramatic advancements have been achieved in the field of MSPs. Before *Fermi*, 70 MSPs were known outside globular clusters; now 120 have been found, 39 of which are part of the 2PC (Abdo et al. 2013). The 40th *Fermi* MSP is J1823-3121A, located within the globular cluster NGC6624, which represents the first detection of gamma-ray pulsations from an MSP in a globular cluster (Freire et al. 2011).

MSPs found in *Fermi* error boxes are a shorter-period, more energetic population than radio-selected ones (Ray et al. 2012). Indeed gamma-ray MSPs dominate for  $P < 0.003$  s. In addition, Roberts (2013) remarks that MSPs found in *Fermi* sources have dramatically increased the number of black widow-type systems where the MSP is driving the evaporation of its tightly-bound very light binary companion.

Thus, the unexpected split into three pulsar classes makes 2PC (Abdo et al. 2013) noteworthy both in quantity and diversity. This is highlighted in **Tables 1–3**, which summarize the parameters of the 117 2PC (Abdo et al. 2013) pulsars divided into radio-loud pulsars, radio quiet pulsars, and MSPs.

When looking at the 2PC (Abdo et al. 2013) numbers, one must also consider the sensitivity issue because different search techniques, as well as different sky locations, do result in different sensitivities. As shown by Dormody et al. (2011), blind searches are about 2.5 times less sensitive than folding gamma rays with a known ephemeris. Thus, the similar number of detections among radio-loud and radio-quiet pulsars tells us that the parent population must contain more radio-quiet pulsars, as expected based on the OG model (e.g., Romani & Yadigaroglu 1995 foresaw that the radio-quiet gamma-ray-emitting INs should account for half of the young NSs, but that only 19% should be visible both in gamma-ray and radio wavelengths).

#### 4.1. The Galactic Distribution of Pulsars Revealed by *Fermi*

Although hard to distinguish from their gamma-ray light curves and spectra, the three pulsar families have markedly different Galactic distributions as well as different average fluxes. The Galactic distribution of the different classes of 2PC (Abdo et al. 2013) pulsars, given in **Figure 5**, clearly shows that young pulsars (both radio-loud and radio-quiet) are clustered around the Galactic plane, where they are much harder to detect owing to higher Galactic background radiation, whereas MSPs (be they gamma-ray pulsars or new radio pulsars discovered in *Fermi*

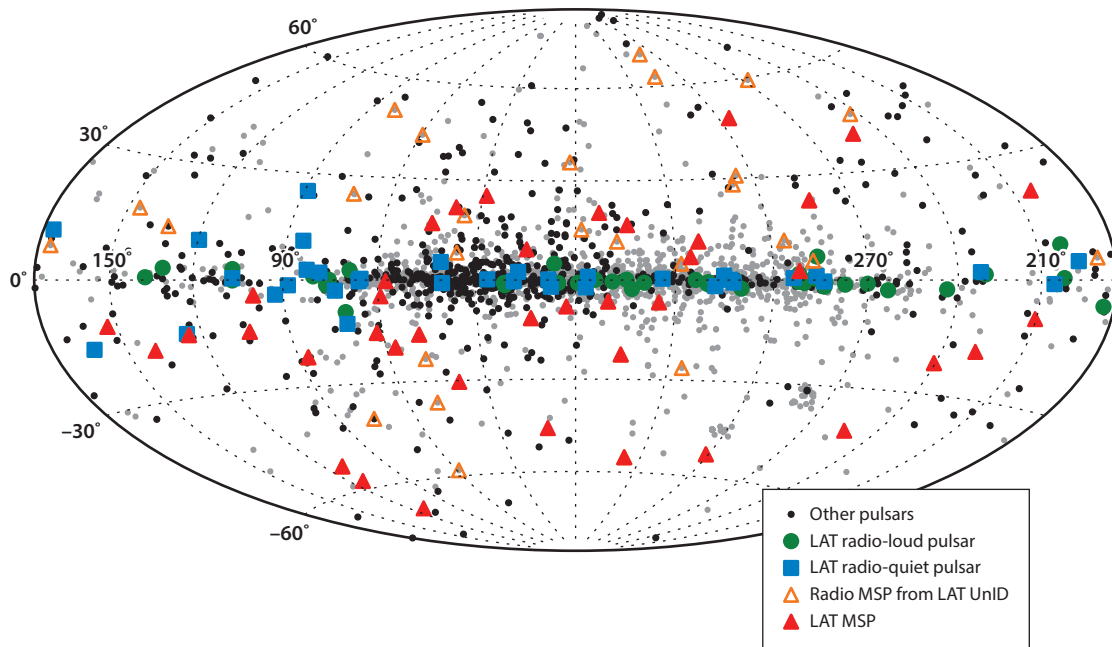


**Figure 5**

The Galactic distribution of 117 *Fermi* pulsars: radio-loud pulsars in green circles, radio-quiet in blue squares, and millisecond pulsars (MSPs) in red triangles. Empty triangles represent radio MSPs discovered within *Fermi* unidentified sources, whereas filled triangles are MSPs detected as gamma-ray pulsars. Black dots indicate 710 radio pulsars that were (unsuccessfully) phase folded with radio ephemerides provided by the Pulsar Timing Consortium. Gray dots indicate 1,337 pulsars outside globular clusters for which phase folding was not performed. Reprinted from 2PC (Abdo et al. 2013) with permission.

error boxes) are distributed all over the sky, pointing to a relatively local origin. However, the paucity of MSPs close to the Galactic plane is probably an observational bias because the *Fermi* unidentified source radio programs preferentially select sources at high Galactic latitude, avoiding regions where gamma-ray diffuse emission is higher and source confusion more likely.

The similarities/differences between the three pulsar classes can be immediately gauged by plotting their  $\log N$ - $\log S$  distributions (see **Figure 6**). Whereas young pulsars (both radio-loud and radio-quiet) have comparable fluxes and a number-flux slope in the range of  $-0.7$  to  $-0.9$ , number-flux distribution of MSPs is definitely steeper (slope =  $-1.6$ ) with a much lower average source flux. According to a straightforward geometric interpretation of the  $\log N$ - $\log S$  plot, a Galactic cylindrical distribution with no boundaries would yield a  $-1$  slope, whereas a homogeneously filled sphere would be characterized by a  $-1.5$  slope. Thus, young pulsars seem to trace a Galactic disk-like population that lacks faint sources, probably owing to the high Galactic background, whereas MSPs point to a spherical distribution of intrinsically fainter sources in our Galactic Neighborhood.

#### 4.2. General Population Properties: Are Radio-Loud Pulsars Different from Radio-Quiet Pulsars?

To put the 117 *Fermi* pulsars in context, it is useful to plot them on the pulsar  $P - \dot{P}$  diagram. This is given in **Figure 7**, extracted from the 2PC (Abdo et al. 2013). At first glance, it is easy to note that all the detections lie above the line corresponding to  $\dot{E} = 10^{33}$  erg  $\text{sec}^{-1}$ , which could

**Table 1** Radio-loud isolated neutron stars

Pulsar name	Galactic latitude (deg)	Galactic longitude (deg)	$P$ (ms)	$\dot{P}$ ( $s\ s^{-1}$ )	$\dot{E}$ ( $\text{erg}\ s^{-1}$ )	Luminosity ( $\text{erg}\ s^{-1}$ )	Distance (kpc)	Age (year)	$B_s$ (G)	$B_{LC}$ (G)	Comments
J0205+6449	130.72	3.08	65.727	$1.90 \times 10^{-13}$	$2.64 \times 10^{37}$	$2.44 \times 10^{34}$	1.95	$5.48 \times 10^3$	$3.58 \times 10^{12}$	$1.16 \times 10^5$	
J0248+6021	136.90	0.70	217.107	$5.50 \times 10^{-14}$	$2.12 \times 10^{35}$	$2.47 \times 10^{34}$	2.0	$6.25 \times 10^4$	$3.50 \times 10^{12}$	$3.15 \times 10^3$	
J0534+2200 (B0531+21)	184.56	-5.78	33.635	$4.20 \times 10^{-13}$	$4.36 \times 10^{38}$	$6.19 \times 10^{35}$	2.0	$1.27 \times 10^3$	$3.80 \times 10^{12}$	$9.21 \times 10^5$	Crab
J0631+1036	201.22	0.45	287.803	$1.05 \times 10^{-13}$	$1.73 \times 10^{35}$	$5.57 \times 10^{33}$	1.0	$4.36 \times 10^4$	$5.55 \times 10^{12}$	$2.14 \times 10^3$	
J0659+1414 (B0656+14)	201.11	8.26	384.919	$5.50 \times 10^{-14}$	$3.81 \times 10^{34}$	$2.35 \times 10^{32}$	0.28	$1.11 \times 10^5$	$4.66 \times 10^{12}$	$7.52 \times 10^2$	
J0729-1448	230.39	1.42	251.691	$1.14 \times 10^{-13}$	$2.82 \times 10^{35}$	$1.72 \times 10^{34}$	3.52	$3.50 \times 10^4$	$5.42 \times 10^{12}$	$3.13 \times 10^3$	
J0742-2822 (B0740-28)	243.77	-2.44	166.771	$1.68 \times 10^{-14}$	$1.43 \times 10^{35}$	$8.89 \times 10^{33}$	2.07	$1.57 \times 10^5$	$1.69 \times 10^{12}$	$3.36 \times 10^3$	
J0835-4510 (B0833-45)	263.55	-2.79	89.365	$1.25 \times 10^{-13}$	$6.90 \times 10^{36}$	$8.93 \times 10^{34}$	0.29	$1.14 \times 10^4$	$3.38 \times 10^{12}$	$4.36 \times 10^4$	Vela
J0908-4913 (B0906-49)	270.27	-1.02	106.755	$1.51 \times 10^{-14}$	$4.90 \times 10^{35}$	$3.50 \times 10^{34}$	2.57	$1.12 \times 10^5$	$1.29 \times 10^{12}$	$9.72 \times 10^3$	
J0940-5428	277.51	-1.29	87.545	$3.28 \times 10^{-14}$	$1.93 \times 10^{36}$	$4.22 \times 10^{33}$	2.95	$4.23 \times 10^4$	$1.71 \times 10^{12}$	$2.35 \times 10^4$	
J1016-5857	284.08	-1.88	107.386	$8.06 \times 10^{-14}$	$2.57 \times 10^{36}$	$5.48 \times 10^{34}$	2.9	$2.11 \times 10^4$	$2.98 \times 10^{12}$	$2.21 \times 10^4$	
J1019-5749	283.84	-0.68	162.506	$2.01 \times 10^{-14}$	$1.84 \times 10^{35}$	$4.27 \times 10^{34}$	6.8	$1.28 \times 10^5$	$1.83 \times 10^{12}$	$3.92 \times 10^3$	
J1028-5819	285.07	-0.50	91.403	$1.61 \times 10^{-14}$	$8.33 \times 10^{35}$	$1.58 \times 10^{35}$	2.33	$8.99 \times 10^4$	$1.23 \times 10^{12}$	$1.48 \times 10^4$	
J1048-5832 (B1046-58)	287.43	0.58	123.701	$9.57 \times 10^{-14}$	$2.00 \times 10^{36}$	$1.76 \times 10^{35}$	2.74	$2.05 \times 10^4$	$3.48 \times 10^{12}$	$1.69 \times 10^4$	
J1057-5226 (B1055-52)	285.98	6.65	197.114	$5.83 \times 10^{-15}$	$3.01 \times 10^{34}$	$4.33 \times 10^{33}$	0.35	$5.35 \times 10^5$	$1.09 \times 10^{12}$	$1.30 \times 10^3$	EGRET
J1105-6107	290.49	-0.85	63.198	$1.58 \times 10^{-14}$	$2.48 \times 10^{36}$	$1.45 \times 10^{35}$	4.98	$6.32 \times 10^4$	$1.01 \times 10^{12}$	$3.69 \times 10^4$	

(Continued)

**Table 1** (Continued)

J1112-6103	291.22	-0.46	64.962	$3.15 \times 10^{-14}$	$4.54 \times 10^{36}$	$3.62 \times 10^{35}$	12.2	$3.27 \times 10^4$	$1.45 \times 10^{12}$	$4.86 \times 10^4$
J1119-6127	292.15	-0.54	408.732	$4.03 \times 10^{-12}$	$2.33 \times 10^{36}$	$6.03 \times 10^{35}$	8.4	$1.61 \times 10^3$	$4.11 \times 10^{13}$	$5.53 \times 10^3$
J1124-5916	292.04	1.75	135.493	$7.50 \times 10^{-13}$	$1.19 \times 10^{37}$	$1.70 \times 10^{35}$	4.8	$2.86 \times 10^3$	$1.02 \times 10^{13}$	$3.78 \times 10^4$
J1337-6429	309.92	-2.51	166.167	$3.57 \times 10^{-13}$	$3.07 \times 10^{36}$	$2.53 \times 10^{34}$	2.5	$7.37 \times 10^3$	$7.80 \times 10^{12}$	$1.56 \times 10^4$
J1410-6132	312.19	-0.09	50.052	$3.18 \times 10^{-14}$	$1.00 \times 10^{37}$	$7.66 \times 10^{35}$	15.6	$2.50 \times 10^4$	$1.28 \times 10^{12}$	$9.37 \times 10^4$
J1420-6048	313.54	0.23	68.202	$8.29 \times 10^{-14}$	$1.03 \times 10^{37}$	$6.39 \times 10^{35}$	5.61	$1.30 \times 10^4$	$2.41 \times 10^{12}$	$6.98 \times 10^4$
J1509-5850	319.97	-0.62	88.925	$9.17 \times 10^{-15}$	$5.15 \times 10^{35}$	$1.05 \times 10^{35}$	2.62	$1.54 \times 10^5$	$9.14 \times 10^{11}$	$1.20 \times 10^4$
J1513-5908 (B1509-58)	320.32	-1.16	151.578	$1.53 \times 10^{-12}$	$1.73 \times 10^{37}$	$6.88 \times 10^{34}$	4.21	$1.57 \times 10^3$	$1.54 \times 10^{13}$	$4.07 \times 10^4$
J1531-5610	323.90	0.03	84.201	$1.38 \times 10^{-14}$	$9.12 \times 10^{35}$	$1.01 \times 10^{33}$	2.09	$9.67 \times 10^4$	$1.09 \times 10^{12}$	$1.68 \times 10^4$
J1648-4611	339.44	-0.79	164.958	$2.37 \times 10^{-14}$	$2.09 \times 10^{35}$	$1.60 \times 10^{35}$	4.96	$1.10 \times 10^5$	$2.00 \times 10^{12}$	$4.11 \times 10^3$
J1702-4128	344.74	0.12	182.153	$5.23 \times 10^{-14}$	$3.42 \times 10^{35}$	$7.67 \times 10^{34}$	4.75	$5.52 \times 10^4$	$3.12 \times 10^{12}$	$4.76 \times 10^3$
J1709-4429 (B1706-44)	343.11	-2.67	102.496	$9.28 \times 10^{-14}$	$3.40 \times 10^{36}$	$8.53 \times 10^{35}$	2.3	$1.75 \times 10^4$	$3.12 \times 10^{12}$	$2.67 \times 10^4$
J1718-3825	348.95	-0.43	74.675	$1.32 \times 10^{-14}$	$1.25 \times 10^{36}$	$1.38 \times 10^{35}$	3.6	$8.98 \times 10^4$	$1.00 \times 10^{12}$	$2.22 \times 10^4$
J1730-3350 (B1727-33)	354.14	0.09	139.497	$8.48 \times 10^{-14}$	$1.23 \times 10^{36}$	$3.56 \times 10^{34}$	3.55	$2.61 \times 10^4$	$3.48 \times 10^{12}$	$1.18 \times 10^4$
J1741-2054	6.42	4.91	413.701	$1.70 \times 10^{-14}$	$9.47 \times 10^{33}$	$2.06 \times 10^{33}$	0.38	$3.86 \times 10^5$	$2.68 \times 10^{12}$	$3.49 \times 10^2$
J1747-2958	359.31	-0.84	98.827	$6.13 \times 10^{-14}$	$2.51 \times 10^{36}$	$5.70 \times 10^{35}$	4.75	$2.55 \times 10^4$	$2.49 \times 10^{12}$	$2.38 \times 10^4$
J1801-2451 (B1757-24)	5.25	-0.89	124.948	$1.27 \times 10^{-13}$	$2.57 \times 10^{36}$	$3.91 \times 10^{34}$	5.22	$1.56 \times 10^4$	$4.03 \times 10^{12}$	$1.90 \times 10^4$
J1833-1034	21.50	-0.89	61.888	$2.02 \times 10^{-13}$	$3.36 \times 10^{37}$	$1.56 \times 10^{35}$	4.7	$4.85 \times 10^3$	$3.58 \times 10^{12}$	$1.39 \times 10^5$
J1835-1106	21.22	-1.51	165.916	$2.06 \times 10^{-14}$	$1.78 \times 10^{35}$	$5.80 \times 10^{33}$	2.83	$1.28 \times 10^5$	$1.87 \times 10^{12}$	$3.77 \times 10^3$
J1952+3252 (B1951+32)	68.77	2.82	39.534	$5.83 \times 10^{-15}$	$3.72 \times 10^{36}$	$6.61 \times 10^{34}$	2.0	$1.07 \times 10^5$	$4.86 \times 10^{11}$	$7.24 \times 10^4$
J2021+3651	75.22	0.11	103.742	$9.56 \times 10^{-14}$	$3.38 \times 10^{36}$	$5.91 \times 10^{36}$	10.0	$1.72 \times 10^4$	$3.19 \times 10^{12}$	$2.63 \times 10^4$
J2030+3641	76.12	-1.44	200.129	$6.51 \times 10^{-15}$	$3.20 \times 10^{34}$	$3.38 \times 10^{34}$	3.0	$4.87 \times 10^5$	$1.15 \times 10^{12}$	$1.33 \times 10^3$
J2032+4127	80.22	1.03	143.248	$2.04 \times 10^{-14}$	$2.73 \times 10^{35}$	$1.69 \times 10^{35}$	3.65	$1.11 \times 10^5$	$1.73 \times 10^{12}$	$5.41 \times 10^3$
J2043+2740	70.61	-9.15	96.131	$1.23 \times 10^{-15}$	$5.46 \times 10^{34}$	$3.83 \times 10^{33}$	1.8	$1.24 \times 10^6$	$3.48 \times 10^{11}$	$3.60 \times 10^3$
J2229+6114	106.65	2.95	51.643	$7.79 \times 10^{-14}$	$2.23 \times 10^{37}$	$1.94 \times 10^{34}$	0.8	$1.05 \times 10^4$	$2.03 \times 10^{12}$	$1.36 \times 10^5$
J2240+5832	106.57	-0.11	139.941	$1.52 \times 10^{-14}$	$2.19 \times 10^{35}$	$7.68 \times 10^{34}$	7.7	$1.46 \times 10^5$	$1.48 \times 10^{12}$	$4.96 \times 10^3$

**Table 2** Radio-quiet isolated neutron stars

Pulsar name	Galactic latitude (deg)	Galactic longitude (deg)	$P$ (ms)	$\dot{P}$ ( $s\ s^{-1}$ )	$\dot{E}$ ( $\text{erg}\ s^{-1}$ )	Luminosity ( $\text{erg}\ s^{-1}$ )	Distance (kpc)	Age (year)	$B_s$ (G)	$B_{JC}$ (G)	Comments
J0007+7303	119.66	10.46	315.893	$3.57 \times 10^{-13}$	$4.48 \times 10^{35}$	$9.39 \times 10^{34}$	1.4	$1.40 \times 10^4$	$1.08 \times 10^{13}$	$3.14 \times 10^3$	CTA-1
J0106+4855	125.47	-13.87	83.157	$4.28 \times 10^{-16}$	$2.94 \times 10^{34}$	$2.09 \times 10^{34}$	3.01	$3.08 \times 10^6$	$1.91 \times 10^{11}$	$3.06 \times 10^3$	
J0357+3205	162.76	-16.01	444.105	$1.31 \times 10^{-14}$	$5.90 \times 10^{33}$	$<5.16 \times 10^{35}$	$<8.2$	$5.37 \times 10^5$	$2.44 \times 10^{12}$	$2.56 \times 10^2$	
J0622+3749	175.88	10.96	333.208	$2.54 \times 10^{-14}$	$2.71 \times 10^{34}$	$<1.19 \times 10^{35}$	$<8.3$	$2.08 \times 10^5$	$2.94 \times 10^{12}$	$7.33 \times 10^2$	
J0633+0632	205.09	-0.93	297.397	$7.96 \times 10^{-14}$	$1.19 \times 10^{35}$	$<8.52 \times 10^{35}$	$<8.7$	$5.92 \times 10^4$	$4.92 \times 10^{12}$	$1.72 \times 10^3$	
J0633+1746	195.13	4.27	237.104	$1.10 \times 10^{-14}$	$3.25 \times 10^{34}$	$3.17 \times 10^{34}$	0.25	$3.42 \times 10^5$	$1.63 \times 10^{12}$	$1.13 \times 10^3$	Geminga
J0734-1559	232.06	2.02	155.141	$1.25 \times 10^{-14}$	$1.32 \times 10^{35}$	$<7.05 \times 10^{35}$	$<10.3$	$1.96 \times 10^5$	$1.41 \times 10^{12}$	$3.48 \times 10^3$	
J1023-5746	284.17	-0.41	111.479	$3.82 \times 10^{-13}$	$1.09 \times 10^{37}$	$<6.58 \times 10^{36}$	$<16.8$	$4.62 \times 10^3$	$6.61 \times 10^{12}$	$4.39 \times 10^4$	
J1044-5737	286.58	1.16	139.030	$5.46 \times 10^{-14}$	$8.02 \times 10^{35}$	$<5.52 \times 10^{36}$	$<17.2$	$4.03 \times 10^4$	$2.79 \times 10^{12}$	$9.55 \times 10^3$	
J1135-6055	293.79	0.58	114.487	$7.84 \times 10^{-14}$	$2.06 \times 10^{36}$	$<1.94 \times 10^{36}$	$<18.4$	$2.31 \times 10^4$	$3.03 \times 10^{12}$	$1.86 \times 10^4$	
J1413-6205	312.37	-0.74	109.741	$2.74 \times 10^{-14}$	$8.18 \times 10^{35}$	$<8.62 \times 10^{36}$	$<21.4$	$6.35 \times 10^4$	$1.75 \times 10^{12}$	$1.22 \times 10^4$	
J1418-6058	313.32	0.13	110.577	$1.69 \times 10^{-13}$	$4.94 \times 10^{36}$	$9.24 \times 10^{34}$	1.6	$1.03 \times 10^4$	$4.38 \times 10^{12}$	$2.98 \times 10^4$	
J1429-5911	315.26	1.30	115.844	$3.05 \times 10^{-14}$	$7.74 \times 10^{35}$	$<4.57 \times 10^{36}$	$<21.8$	$6.02 \times 10^4$	$1.90 \times 10^{12}$	$1.13 \times 10^4$	
J1459-6053	317.89	-1.79	103.151	$2.53 \times 10^{-14}$	$9.09 \times 10^{35}$	$<7.62 \times 10^{36}$	$<22.2$	$6.47 \times 10^4$	$1.63 \times 10^{12}$	$1.37 \times 10^4$	
J1620-4927	333.89	0.41	171.935	$1.05 \times 10^{-14}$	$8.15 \times 10^{34}$	$<1.08 \times 10^{37}$	$<24.1$	$2.60 \times 10^5$	$1.36 \times 10^{12}$	$2.46 \times 10^3$	
J1732-3131	356.31	1.01	196.544	$2.80 \times 10^{-14}$	$1.46 \times 10^{35}$	$8.62 \times 10^{33}$	0.61	$1.11 \times 10^5$	$2.38 \times 10^{12}$	$2.88 \times 10^3$	
J1746-3239	356.96	-2.17	199.541	$6.56 \times 10^{-15}$	$3.26 \times 10^{34}$	$<5.53 \times 10^{36}$	$<25.3$	$4.82 \times 10^5$	$1.16 \times 10^{12}$	$1.34 \times 10^3$	
J1803-2149	8.14	0.19	106.332	$1.95 \times 10^{-14}$	$6.41 \times 10^{35}$	$<7.01 \times 10^{36}$	$<25.2$	$8.63 \times 10^4$	$1.46 \times 10^{12}$	$1.12 \times 10^4$	
J1809-2332	7.39	-1.99	146.789	$3.44 \times 10^{-14}$	$4.30 \times 10^{35}$	$1.64 \times 10^{35}$	1.7	$6.76 \times 10^4$	$2.27 \times 10^{12}$	$6.62 \times 10^3$	Taz
J1813-1246	17.24	2.44	48.073	$1.76 \times 10^{-14}$	$6.24 \times 10^{36}$	$<1.84 \times 10^{37}$	$<24.7$	$4.34 \times 10^4$	$9.30 \times 10^{11}$	$7.70 \times 10^4$	
J1826-1256	18.56	-0.38	110.227	$1.21 \times 10^{-13}$	$3.58 \times 10^{36}$	$<2.79 \times 10^{37}$	$<24.7$	$1.44 \times 10^4$	$3.70 \times 10^{12}$	$2.54 \times 10^4$	El

(Continued)

**Table 2** (Continued)

J1836+5925	88.88	25.00	173.264	$1.50 \times 10^{-15}$	$1.14 \times 10^{34}$	$2.04 \times 10^{34}$	0.53	$1.83 \times 10^6$	$5.16 \times 10^{11}$	$9.14 \times 10^7$	Next Geminga
J1838+0337	26.51	0.21	145.709	$4.65 \times 10^{-13}$	$5.93 \times 10^{36}$	$<1.30 \times 10^{37}$	$<24.1$	$4.97 \times 10^3$	$8.33 \times 10^{12}$	$2.48 \times 10^4$	
J1846+0919	40.69	5.34	225.552	$9.93 \times 10^{-15}$	$3.42 \times 10^{34}$	$<1.40 \times 10^{36}$	$<22.0$	$3.60 \times 10^5$	$1.51 \times 10^{12}$	$1.21 \times 10^3$	
J1907+0602	40.18	-0.89	106.636	$8.67 \times 10^{-14}$	$2.82 \times 10^{36}$	$3.14 \times 10^{35}$	3.21	$1.95 \times 10^4$	$3.08 \times 10^{12}$	$2.34 \times 10^4$	
J1954+2836	65.24	0.38	92.710	$2.12 \times 10^{-14}$	$1.05 \times 10^{36}$	$<4.28 \times 10^{36}$	$<18.6$	$6.94 \times 10^4$	$1.42 \times 10^{12}$	$1.64 \times 10^4$	
J1957+5033	84.60	11.00	374.806	$6.83 \times 10^{-15}$	$5.12 \times 10^{33}$	$<6.59 \times 10^{33}$	$<14.5$	$8.69 \times 10^5$	$1.62 \times 10^{12}$	$2.83 \times 10^2$	
J1958+2846	65.88	-0.35	290.397	$2.12 \times 10^{-13}$	$3.42 \times 10^{35}$	$<3.74 \times 10^{36}$	$<18.5$	$2.17 \times 10^4$	$7.94 \times 10^{12}$	$2.98 \times 10^3$	
J2021+4026	78.23	2.09	265.320	$5.42 \times 10^{-14}$	$1.14 \times 10^{35}$	$2.57 \times 10^{35}$	1.5	$7.76 \times 10^4$	$3.84 \times 10^{12}$	$1.89 \times 10^3$	$\gamma$ Cygni
J2028+3332	73.36	-3.01	176.707	$4.86 \times 10^{-15}$	$3.48 \times 10^{34}$	$<2.06 \times 10^{36}$	$<17.2$	$5.76 \times 10^5$	$9.37 \times 10^{11}$	$1.56 \times 10^3$	
J2030+4415	82.34	2.89	227.070	$6.49 \times 10^{-15}$	$2.19 \times 10^{34}$	$<1.69 \times 10^{36}$	$<15.7$	$5.54 \times 10^5$	$1.23 \times 10^{12}$	$9.66 \times 10^2$	
J2055+2559	70.69	-12.52	319.561	$4.11 \times 10^{-15}$	$4.97 \times 10^{33}$	$<1.50 \times 10^{36}$	$<15.3$	$1.23 \times 10^6$	$1.16 \times 10^{12}$	$3.27 \times 10^2$	
J2111+4606	88.31	-1.45	157.830	$1.43 \times 10^{-13}$	$1.44 \times 10^{36}$	$<1.15 \times 10^{36}$	$<14.8$	$1.75 \times 10^4$	$4.81 \times 10^{12}$	$1.13 \times 10^4$	
J2139+4716	92.63	-4.02	282.849	$1.80 \times 10^{-15}$	$3.15 \times 10^{33}$	$<5.56 \times 10^{35}$	$<14.1$	$2.49 \times 10^6$	$7.23 \times 10^{11}$	$2.94 \times 10^2$	
J2238+5903	106.56	0.48	162.734	$9.70 \times 10^{-14}$	$8.88 \times 10^{35}$	$<1.18 \times 10^{36}$	$<12.4$	$2.66 \times 10^4$	$4.02 \times 10^{12}$	$8.59 \times 10^3$	

**Table 3** Millisecond pulsars

Pulsar name	Galactic latitude (deg)	Galactic longitude (deg)	$P$ (ms)	$\dot{P}$ ( $s\ s^{-1}$ )	$\dot{E}$ ( $\text{erg}\ s^{-1}$ )	Luminosity ( $\text{erg}\ s^{-1}$ )	Distance (kpc)	Age (year)	$B_s$ (G)	$B_{1C}$ (G)	Comments
J0023+0923	111.38	-52.85	3.050	$1.09 \times 10^{-20}$	$1.51 \times 10^{34}$	$4.56 \times 10^{32}$	0.69	$4.45 \times 10^9$	$1.84 \times 10^8$	$5.97 \times 10^4$	
J0030+0451	113.14	-57.61	4.870	$1.02 \times 10^{-20}$	$3.62 \times 10^{33}$	$5.75 \times 10^{32}$	0.28	$7.28 \times 10^9$	$2.30 \times 10^8$	$1.83 \times 10^4$	
J0034-0534	111.49	-68.07	1.880	$4.98 \times 10^{-21}$	$1.72 \times 10^{34}$	$5.67 \times 10^{32}$	0.54	$1.03 \times 10^{10}$	$7.46 \times 10^7$	$1.03 \times 10^5$	
J0101-6422	301.19	-52.72	2.570	$4.80 \times 10^{-21}$	$1.01 \times 10^{34}$	$3.79 \times 10^{32}$	0.55	$9.42 \times 10^9$	$1.07 \times 10^8$	$5.79 \times 10^4$	
J0102+4839	124.87	-14.17	2.960	$1.17 \times 10^{-20}$	$1.75 \times 10^{34}$	$8.51 \times 10^{33}$	2.32	$4.01 \times 10^9$	$1.88 \times 10^8$	$6.68 \times 10^4$	
J0218+4232	139.51	-17.53	2.320	$7.74 \times 10^{-20}$	$2.43 \times 10^{35}$	$3.80 \times 10^{34}$	2.64	$4.78 \times 10^8$	$4.27 \times 10^8$	$3.15 \times 10^5$	
J0340+4130	153.78	-11.02	3.300	$5.90 \times 10^{-21}$	$7.87 \times 10^{33}$	$7.29 \times 10^{33}$	1.73	$8.86 \times 10^9$	$1.41 \times 10^8$	$3.62 \times 10^4$	
J0437-4715	253.39	-41.96	5.760	$5.73 \times 10^{-20}$	$2.91 \times 10^{33}$	$4.86 \times 10^{31}$	0.16	$6.49 \times 10^9$	$2.88 \times 10^8$	$1.39 \times 10^4$	
J0610-2100	227.75	-18.18	3.860	$1.23 \times 10^{-20}$	$8.35 \times 10^{32}$	$9.85 \times 10^{33}$	3.54	$5.03 \times 10^{10}$	$6.93 \times 10^7$	$1.11 \times 10^4$	
J0613-0200	210.41	-9.30	3.060	$9.59 \times 10^{-21}$	$1.20 \times 10^{34}$	$2.90 \times 10^{33}$	0.9	$5.55 \times 10^9$	$1.65 \times 10^8$	$5.31 \times 10^4$	
J0614-3329	240.50	-21.83	3.150	$1.78 \times 10^{-20}$	$2.20 \times 10^{34}$	$4.72 \times 10^{34}$	1.9	$2.80 \times 10^9$	$2.40 \times 10^8$	$7.06 \times 10^4$	
J0751+1807	202.73	21.09	3.480	$7.78 \times 10^{-21}$	$7.21 \times 10^{33}$	$2.54 \times 10^{32}$	0.4	$7.16 \times 10^9$	$1.66 \times 10^8$	$3.62 \times 10^4$	
J1024-0719	251.70	40.52	5.160	$1.85 \times 10^{-20}$	$4.60 \times 10^{32}$	$5.67 \times 10^{31}$	0.39	$5.10 \times 10^{10}$	$9.20 \times 10^7$	$6.17 \times 10^3$	
J1124-3653	284.10	22.76	2.410	$5.75 \times 10^{-21}$	$1.71 \times 10^{34}$	$4.29 \times 10^{33}$	1.72	$6.64 \times 10^9$	$1.19 \times 10^8$	$7.83 \times 10^4$	
J1125-5825	291.89	2.60	3.100	$6.09 \times 10^{-20}$	$8.05 \times 10^{34}$	$7.31 \times 10^{33}$	2.62	$8.06 \times 10^8$	$4.40 \times 10^8$	$1.36 \times 10^5$	
J1231-1411	295.53	48.39	3.680	$2.12 \times 10^{-20}$	$5.15 \times 10^{33}$	$2.36 \times 10^{33}$	0.43	$8.98 \times 10^9$	$1.56 \times 10^8$	$2.89 \times 10^4$	
J1446-4701	322.50	11.43	2.190	$9.85 \times 10^{-21}$	$3.68 \times 10^{34}$	$1.89 \times 10^{33}$	1.46	$3.52 \times 10^9$	$1.49 \times 10^8$	$1.30 \times 10^5$	
J1514-4946	325.25	6.81	3.590	$1.87 \times 10^{-20}$	$1.60 \times 10^{34}$	$4.76 \times 10^{33}$	0.94	$3.04 \times 10^9$	$2.62 \times 10^8$	$5.22 \times 10^4$	
J1600-3053	344.09	16.45	3.600	$9.50 \times 10^{-21}$	$7.30 \times 10^{33}$	$1.68 \times 10^{33}$	1.63	$6.61 \times 10^9$	$1.78 \times 10^8$	$3.52 \times 10^4$	
J1614-2230	352.64	20.19	3.150	$9.62 \times 10^{-21}$	$6.33 \times 10^{33}$	$1.23 \times 10^{33}$	0.65	$9.96 \times 10^9$	$1.27 \times 10^8$	$3.74 \times 10^4$	
J1658-5324	334.87	-6.63	2.440	$1.10 \times 10^{-20}$	$3.02 \times 10^{34}$	$2.99 \times 10^{33}$	0.93	$3.51 \times 10^9$	$1.66 \times 10^8$	$1.05 \times 10^5$	
J1713+0747	28.75	25.22	4.570	$8.53 \times 10^{-21}$	$3.44 \times 10^{33}$	$1.34 \times 10^{33}$	1.05	$8.72 \times 10^9$	$1.97 \times 10^8$	$1.90 \times 10^4$	
J1741+1351	37.89	21.64	3.750	$3.02 \times 10^{-20}$	$2.18 \times 10^{34}$	$3.36 \times 10^{32}$	1.08	$2.04 \times 10^9$	$3.34 \times 10^8$	$5.83 \times 10^4$	
J1744-1134	14.79	9.18	4.070	$8.92 \times 10^{-21}$	$4.11 \times 10^{33}$	$6.76 \times 10^{32}$	0.41	$9.19 \times 10^9$	$1.71 \times 10^8$	$2.33 \times 10^4$	
J1747-4036	350.21	-6.41	1.650	$1.33 \times 10^{-20}$	$1.17 \times 10^{35}$	$1.36 \times 10^{34}$	3.39	$1.97 \times 10^9$	$1.50 \times 10^8$	$3.07 \times 10^5$	

(Continued)

Table 3 (Continued)

J1810+1744	44.64	16.81	1.660	$4.63 \times 10^{-21}$	$3.97 \times 10^{34}$	$1.12 \times 10^{34}$	2.0	$5.68 \times 10^9$	$8.87 \times 10^7$	$1.78 \times 10^5$
J1823-3021A (B1820-30A)	2.79	-7.91	5.440	$3.38 \times 10^{-18}$	$8.28 \times 10^{35}$	$7.39 \times 10^{34}$	7.6	$2.55 \times 10^7$	$4.34 \times 10^9$	$2.48 \times 10^5$
J1858-2216	13.58	-11.39	2.380	$3.87 \times 10^{-21}$	$1.13 \times 10^{34}$	$7.64 \times 10^{32}$	0.94	$9.74 \times 10^9$	$9.71 \times 10^7$	$6.63 \times 10^4$
J1902-5105	345.65	-22.38	1.740	$9.00 \times 10^{-21}$	$6.86 \times 10^{34}$	$3.59 \times 10^{33}$	1.18	$3.06 \times 10^9$	$1.27 \times 10^8$	$2.21 \times 10^5$
J1939+2134 (B1937+21)	57.51	-0.29	1.560	$1.05 \times 10^{-19}$	$1.10 \times 10^{36}$	$1.39 \times 10^{34}$	3.56	$2.34 \times 10^8$	$4.10 \times 10^8$	$9.95 \times 10^5$
J1959+2048 (B1957+20)	59.20	-4.70	1.610	$1.68 \times 10^{-20}$	$7.63 \times 10^{34}$	$1.26 \times 10^{34}$	2.49	$3.16 \times 10^9$	$1.15 \times 10^8$	$2.54 \times 10^5$
J2017+0603	48.62	-16.03	2.900	$8.30 \times 10^{-21}$	$1.30 \times 10^{34}$	$9.82 \times 10^{33}$	1.57	$5.54 \times 10^9$	$1.57 \times 10^8$	$5.93 \times 10^4$
J2043+1711	61.92	-15.31	2.380	$5.70 \times 10^{-21}$	$1.27 \times 10^{34}$	$1.00 \times 10^{34}$	1.76	$8.73 \times 10^9$	$1.03 \times 10^8$	$7.01 \times 10^4$
J2047+1053	57.05	-19.68	4.290	$2.10 \times 10^{-20}$	$1.05 \times 10^{34}$	$3.10 \times 10^{33}$	2.05	$3.24 \times 10^9$	$3.04 \times 10^8$	$3.54 \times 10^4$
J2051-0827	39.19	-30.41	4.510	$1.28 \times 10^{-20}$	$5.42 \times 10^{33}$	$4.37 \times 10^{32}$	1.04	$5.68 \times 10^9$	$2.41 \times 10^8$	$2.42 \times 10^4$
J2124-3358	10.93	-45.44	4.930	$2.06 \times 10^{-20}$	$3.67 \times 10^{33}$	$3.96 \times 10^{32}$	0.3	$7.01 \times 10^9$	$2.37 \times 10^8$	$1.82 \times 10^4$
J2214+3000	86.86	-21.67	3.120	$1.50 \times 10^{-20}$	$1.92 \times 10^{34}$	$9.29 \times 10^{33}$	1.54	$3.30 \times 10^9$	$2.19 \times 10^8$	$6.63 \times 10^4$
J2215+5135	99.87	-4.16	2.610	$2.34 \times 10^{-20}$	$5.19 \times 10^{34}$	$1.28 \times 10^{34}$	3.01	$1.77 \times 10^9$	$2.50 \times 10^8$	$1.29 \times 10^5$
J2241-5236	337.46	-54.93	2.190	$8.70 \times 10^{-21}$	$2.60 \times 10^{34}$	$1.05 \times 10^{33}$	0.51	$3.99 \times 10^9$	$1.40 \times 10^8$	$1.22 \times 10^5$
J2302+4442	103.40	-14.00	5.190	$1.33 \times 10^{-20}$	$3.82 \times 10^{33}$	$6.21 \times 10^{33}$	1.19	$6.18 \times 10^9$	$2.66 \times 10^8$	$1.75 \times 10^4$

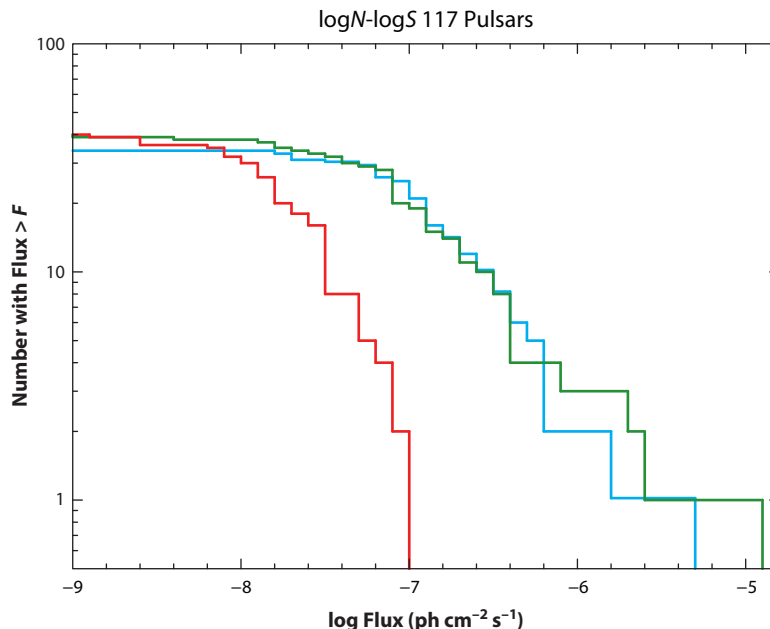


**Figure 6**

A  $\log N$ - $\log S$  plot for the three classes of gamma-ray pulsars: radio-loud pulsars are indicated by the green line, radio-quiet pulsars by the blue line, and millisecond pulsars by the red line.

represent either an observational bias or a true death line for gamma-ray pulsar emission. Among the young gamma-ray pulsars a “segregation” effect is seen, with radio-quiet INSs dominating the  $\dot{E}$  interval ranging from  $10^{33}$  to  $10^{35}$  erg sec $^{-1}$ , whereas the opposite is true for  $\dot{E} > 10^{37}$  erg sec $^{-1}$ , where only 1 of the 9 pulsars detected by *Fermi* is radio-quiet. This feature, first noted by Ravi et al. (2010), can be linked to the radio and gamma-ray beaming factors. For high- $\dot{E}$  pulsars the beams should be similar both in sky coverage and in location, and they should be rather high in the pulsar magnetosphere, whereas for low- $\dot{E}$  pulsars the radio-emitting region should migrate toward the NS surface, thus shrinking the sky coverage of the radio beam and resulting in a higher percentage of radio-quiet INSs. Such a beaming evolution is also discussed by Watters & Romani (2011) in their population synthesis simulation.

To understand the *Fermi* pulsars, one of the key parameters seems to be the magnetic field at the light cylinder. As we have already remarked, though the surface B-field of young pulsars is  $10^4$  higher than that inferred for old, recycled ones, the different sizes of their corotating magnetospheres result in a similar B-field at the light cylinder. This is shown in **Figure 8**, where the value of the magnetic field at the light cylinder is plotted against the characteristic age of the pulsars. Once more, the radio-loud/radio-quiet segregation is apparent with the majority of the middle-aged “young” pulsars being radio-quiet, whereas the opposite is true for very young pulsars. Such an effect could result from an observational bias hampering the detection of young, but far-away and thus faint, radio-quiet, very young pulsars. However, if true, such behavior could also be interpreted in the framework of the migration of the radio beaming described above, whereby older and less energetic pulsars are more likely to be spotted as gamma-ray emitters, rather than radio pulsars.

A similar segregation is also seen in the young pulsar spectral parameters. All 117 2PC (Abdo et al. 2013) pulsars have been fitted in a consistent way using a power law with exponential cutoff spectrum. For each pulsar, a power-law index, as well as a value for the cutoff energy, has been

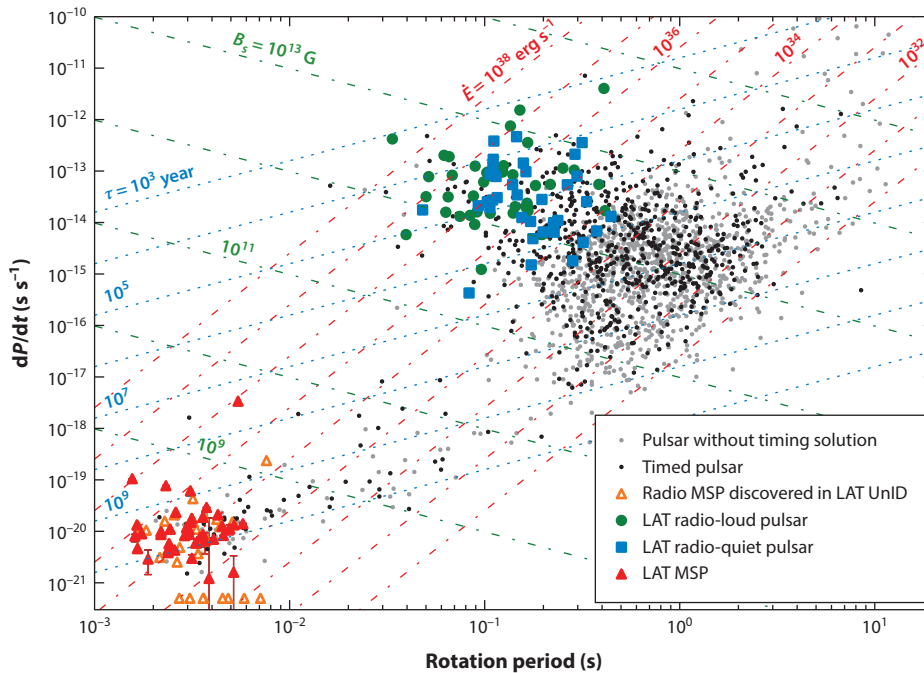


**Figure 7**

$P - \dot{P}$  distribution of the 117 *Fermi* pulsars [radio-loud pulsars shown as green circles, radio-quiet as blue squares, and millisecond pulsars (MSPs) as red triangles] plotted together with the entire radio pulsar sample known today (black dots, 710 in all, represent timed pulsars that were phase folded, but not detected, whereas 1,337 gray dots represent pulsars without timing solution). Lines of constant rotational energy loss ( $\dot{E}_{\text{rot}} = -4\pi^2 IP \dot{P}^{-3}$ ), characteristic age ( $\tau_c = \frac{P}{2\dot{P}}$ ), and surface  $B$  field ( $B_s = (1.5Ic^3 P \dot{P})^{1/2} / 2\pi R_{\text{NS}}^3$ ) are also shown. Recently discovered MSPs, for which no  $\dot{P}$  has been measured, are plotted at  $\dot{P} = 5 \times 10^{-22}$ . All the *Fermi* LAT pulsars lie above  $\dot{E} = 10^{33}$  erg sec $^{-1}$ . Reprinted from 2PC (Abdo et al. 2013) with permission.

computed. Although the power-law indices inferred for MSPs and young pulsars do show positive correlations with their rotational energy losses, when one plots the cutoff energy as a function of the magnetic field at the light cylinder (as in **Figure 9**), radio-quiet pulsars dominate in the region characterized by low cutoff and low magnetic field.

A further effort to characterize radio-loud versus radio-quiet INs has been done through their X-ray emission. A thorough analysis of all the X-ray data available for *Fermi* pulsars has been performed [Marelli et al. 2011, Marelli 2012; later updated within the 2PC (Abdo et al. 2013)] to search for correlation (if any) between the distance independent ratio  $F_\gamma/F_x$  (gamma-ray flux over X-ray flux) and the pulsar age. As there is significant spread in the  $F_\gamma/F_x$  values that spans 3–4 orders of magnitude for objects of similar age and energetics, no correlation was found, although inspection of the X-ray flux data revealed that radio-quiet pulsars tend to be underluminous in X-rays.

### 4.3. The Efficiencies of Gamma-Ray Pulsars: Aged to Perfection

Plotting the gamma-ray luminosity as a function of rotational energy loss of pulsars does not yield a clear picture. Although the plot (shown in **Figure 10**) is hampered by the lack of distance estimates for the majority of radio-quiet NSs, a different trend is apparent for the young pulsars

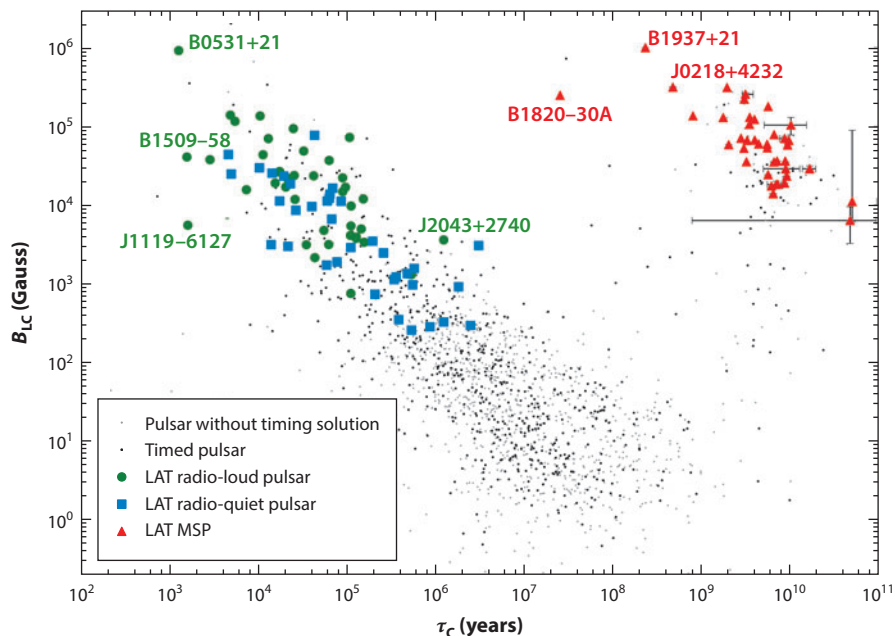


**Figure 8**

The magnetic field at the light cylinder  $B_{LC} = 4\pi^2(1.5I\dot{P})^{1/2}(c^3P^5)^{-1/2}$  is plotted against the isolated neutron star characteristic age  $\tau_c = \frac{P}{2\dot{P}}$ . Radio-loud and radio-quiet pulsars (green circles and blue squares, respectively) are distributed between  $10^2$  and  $10^6$  G, whereas millisecond pulsars (MSPs, red triangles) are more clustered in the  $10^4$ – $10^6$  G region. Courtesy of David Smith, using data from 2PC (Abdo et al. 2013).

as opposed to the old, recycled ones. Though young pulsars seem to follow a  $\sqrt{\dot{E}}$  trend, MSPs prefer a steeper function, pointing to a proportionality between  $L_\gamma$  and  $\dot{E}$ . However, the presence of considerable scattering should not be overlooked. It is probably due to the combination of distance uncertainty with the assumption of a common  $f_\Omega = 1$ . The latter assumption is generally considered acceptable for an outer-magnetosphere fan-like beam(s) sweeping the entire sky. But it has been questioned by Pierbattista et al. (2012), who found a large spread of  $f_\Omega$  among the different emission models and, in more general terms, between radio-loud and radio-quiet pulsars. Clearly, an  $f_\Omega$  value optimized for each pulsar using the model yielding the best fit for its light curve would be highly desirable.

However, when plotting the *Fermi* gamma-ray efficiency (i.e., the ratio between the gamma-ray luminosity and the pulsar rotational energy loss  $L_\gamma/\dot{E}$ ) as a function of the pulsar rotational energy loss as in **Figure 11**, a clear trend appears, showing that old pulsars, which can count on a much smaller energy reservoir, are more efficient in converting their rotational energy loss into gamma rays.

#### 4.4. Do Gamma-Quiet Pulsars Exist?

So far we have discussed the characteristics of the INs detected by *Fermi*. What about those not seen? The point is a nontrivial one because, given the beamed nature of the pulsar emission, it is natural to expect a geometric configuration such that radio emission is detected but gamma-ray pulsation is not. According to Romani & Yadigaroglu (1995), for instance, 8% of the pulsar

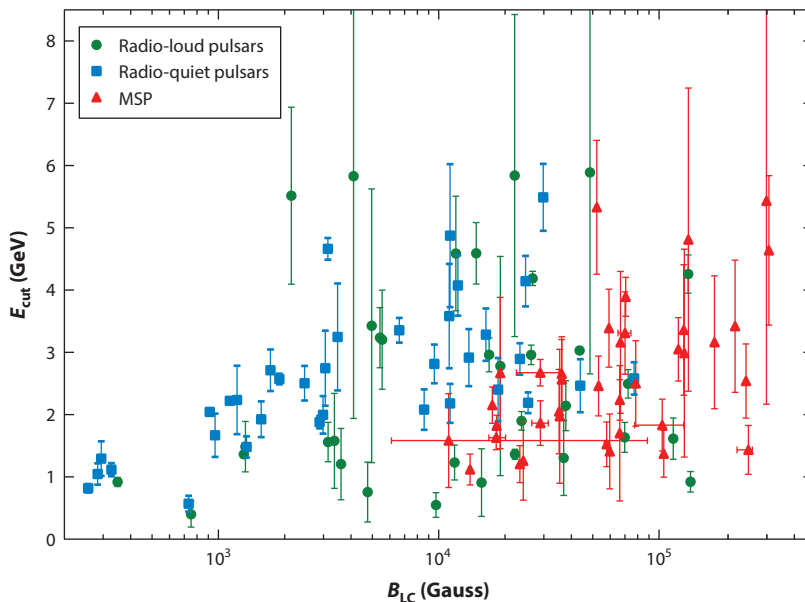


**Figure 9**

Cutoff energy as a function of the magnetic field at the light cylinder. Radio-loud pulsars are shown as *green circles*, radio-quiet as *blue squares*, and millisecond pulsars (MSPs) as *red triangles*. Courtesy of David Smith, using data from 2PC (Abdo et al. 2013).

population should be gamma-ray quiet. Guillemot & Tauris (2014) find that the most energetic MSPs may go undetected in gamma rays owing to unfavorable geometry.

Are there pulsars highly ranked on the basis of  $\frac{\sqrt{\dot{E}}}{4\pi d^2}$  that are not detected by *Fermi*? 28 of the 64 known radio pulsars with  $\dot{E} > 10^{36}$  erg sec<sup>-1</sup> have not been detected and, comparing their upper limits with the “expected” flux (on the basis of their ranking), a number of interesting gamma-quiet candidates appear to be present. However, as discussed in 2PC (Abdo et al. 2013) as well as by Romani et al. (2011), distance uncertainties, confusion with nearby sources, and the possible presence of significant timing noise make it difficult to provide a clear-cut answer. A few INSs have expected gamma-ray flux values well above the current upper limits, but none is yet recognized as a fully convincing gamma-quiet radio pulsar.

#### 4.5. Light Curves and Their Interpretation

Upon inspecting the light curves of the 117 gamma-ray pulsars, one immediately realizes that the majority of the pulsars (70% of the young pulsars and 60% of the MSPs) have two peaks (respectively, *P1* and *P2*, where *P1* is defined as the one soonest in phase after the radio main peak), and that the ratio *P2/P1* increases with energy, indicating a harder second peak. Many double-peaked pulsars display a crescent-type light curve with significant emission between the two peaks. For the Crab and Vela, a third peak emerges from the interpeak bridge emission. However, the third peak of Vela is seen to move in phase as a function of energy (Abdo et al. 2010e), an effect not expected in the current geometric models.

For the radio pulsars, the lag between the radio signal and *P1* is carefully evaluated because it is one of the important parameters in characterizing a pulsar’s multiwavelength behavior. Indeed,

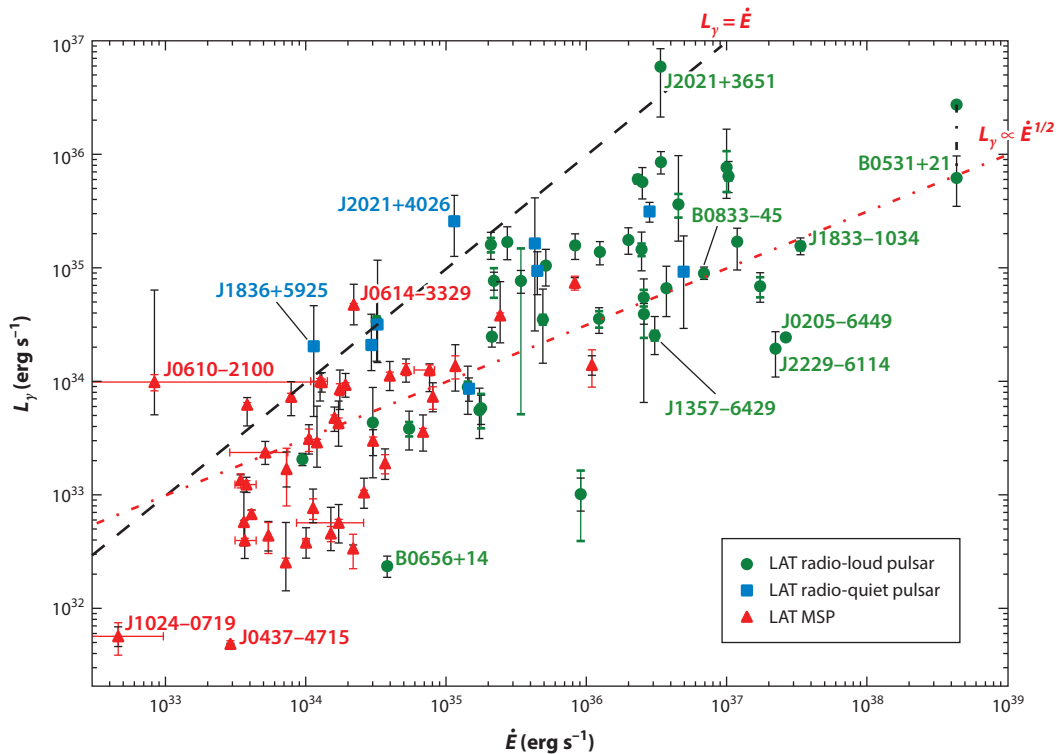


**Figure 10**

Gamma-ray luminosity ( $L_\gamma = 4\pi d^2 F_\gamma f_\Omega$ , computed assuming  $f_\Omega = 1$ ) as a function of the rotational energy loss. The difference in slope between the red cloud of millisecond pulsars (MSPs, *triangles*) and the green cloud of radio-loud pulsars (*circles*) is evident. The paucity of radio-quiet pulsars (*squares*) is due to the lack of distance information. A dashed line represents  $L_\gamma = \dot{E}$ , a rather extreme case used to highlight pulsars whose distances must be significantly overestimated or that require a much narrower beaming factor. A dash-dotted line follows  $\sqrt{\dot{E}}$ . The Crab pulsar, PSR B0531+21, is the only pulsar detected as a very bright X-ray source. The lower point represents the gamma-ray luminosity of the Crab pulsar, whereas the upper point indicates the total luminosity including X-rays. Reprinted from 2PC, Abdo et al. (2013) with permission.

the lag between the radio peak and  $P1$  is greater for MSPs than for young INs, indicating that a smaller magnetosphere implies a stronger aberration of the radio pulses.

Such a wealth of information on pulsar light curves represents a new challenge for theoreticians who try to constrain the geometry of pulsars as well as the relevant magnetospheric physics. Starting from the location(s) of the emitting region(s), namely PC, OG, and SG, or its variation TPC, in a dipole geometry, one can build an “atlas” of predicted gamma-ray light curves to compare to observations. The computed light curves are sensitive to both the magnetic axis inclination ( $\alpha$ ) and the viewing angle ( $\zeta$ ), and with no a priori knowledge on such variables, all the combinations should be considered. **Figure 12** provides an example of emission pattern phase plots computed for a given magnetic inclination ( $\alpha = 45^\circ$ ) for all possible viewing angles. The actual pulsar light curve, obtained cutting the phase plot for a definite value of  $\zeta$ , can be used to select the best fitting value of  $\zeta$  on the basis of the different models. Conversely, external inputs, such as radio polarization angle or X-ray morphological study, can help to constrain the parameter space. The first gamma-ray atlas was compiled by Watters et al. (2009) for vacuum dipole field geometries. Bai & Spitkovsky (2010) considered numerically modeled force-free geometries, whereas Venter

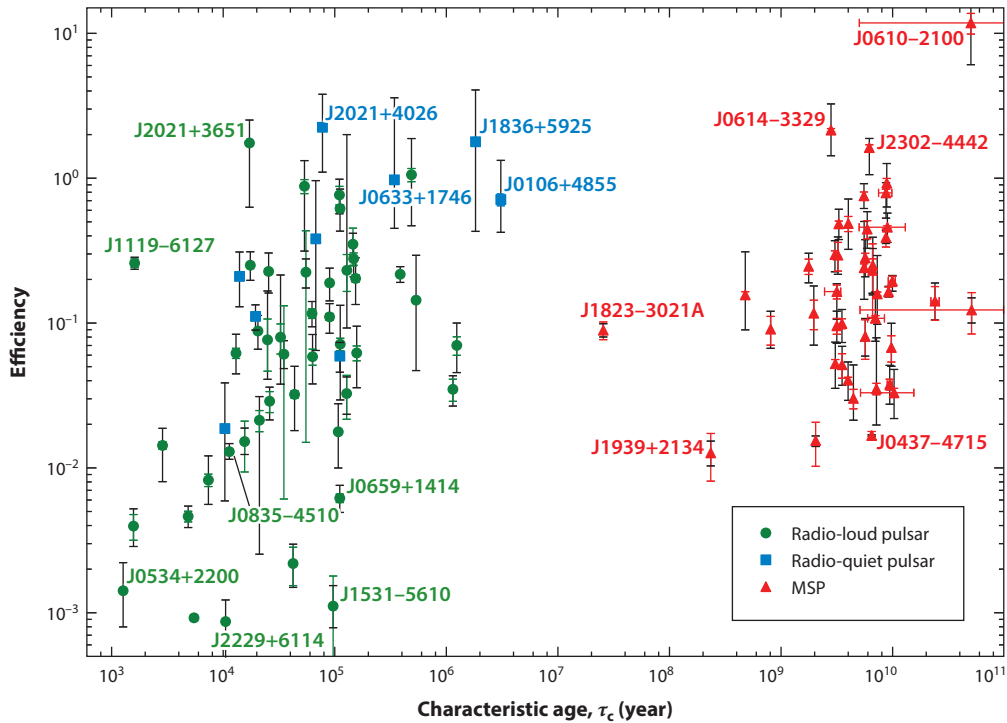


**Figure 11**

Gamma-ray efficiency ( $L_\gamma/\dot{E}$ ) plotted as a function of a pulsar's characteristic age, showing that older and less energetic pulsars are more efficient in converting their rotational energy loss into high-energy gamma rays. Radio-loud pulsars are shown as green circles, radio-quiet pulsars as blue squares, and millisecond pulsars (MSPs) as red triangles. The number of pulsars with an efficiency near or above 1 is to be ascribed to overestimated distances as well as to a too-large beaming factor (here assumed to be 1 for all pulsars). Such a hidden beaming uncertainty is certainly responsible for the unrealistically high efficiency computed for Geminga (J0633+1746), for which the distance is well known. Courtesy of David Smith, using data from 2PC (Abdo et al. 2013).

et al. (2009) concentrated on the newly established MSPs, focusing on their higher percentage of alignment between radio and gamma-ray light curves (Venter et al. 2012). In general, OG models yield better fits (Romani & Watters 2010), but they are not able to account for all the detected pulsars. Lower-altitude emission is preferred for a sizable minority of pulsars, especially those MSPs with aligned radio and gamma-ray light curves. In parallel, emission beyond the light cylinder continues to be a viable alternative (as discussed by Petri 2011).

Pierbattista (2010) extended the atlas approach to also include radio light curves by trying to constrain the  $\alpha$  and  $\zeta$  parameters on the basis of a joint radio-gamma fit. Although promising, the procedure still needs fine-tuning in order to avoid being driven by the radio data. Once a comprehensive gamma-ray and radio light curve atlas is in hand, it can be used to synthesize a pulsar population to be compared with the *Fermi* findings (Pierbattista et al. 2012).

Not surprisingly, the OG model, with its extended beams, can easily account for the observed number of *Fermi* detections while the narrow PC beams can only account for a few pulsars, and the SG need a boost in efficiency to account for the observed set of LAT detections. The population synthesis, however, fails to reproduce the LAT results for high  $\dot{E}$  pulsars. All the models predict too few high  $\dot{E}$  pulsars and cannot explain the high probability of detecting energetic radio-loud pulsars.

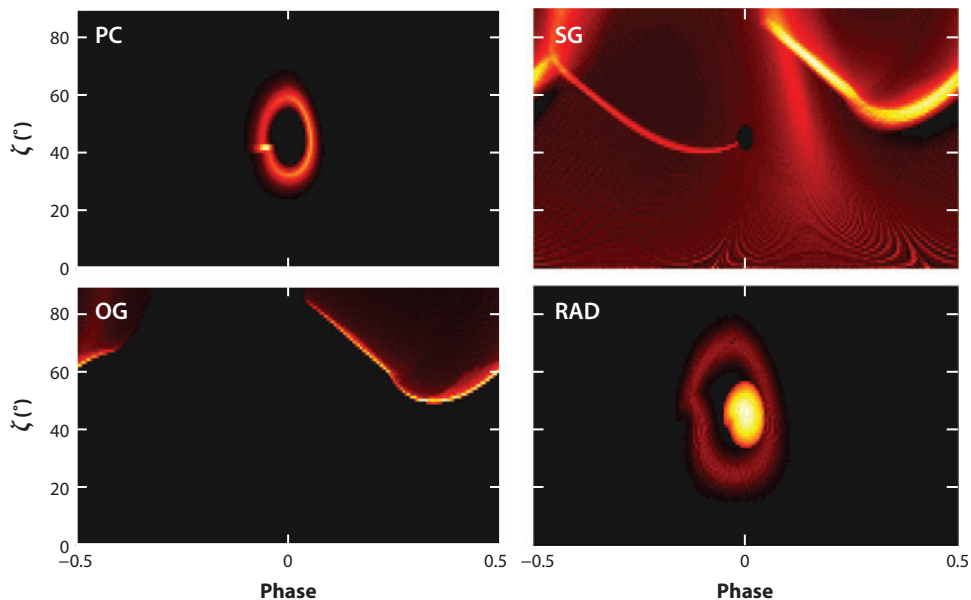


**Figure 12**

Emission pattern phase-plots computed, respectively, for polar cap (PC), slot gap (SG), outer gap (OG), and radio core plus cone models (RAD). For PC and radio models the phase-plots have been obtained for a magnetic field  $B = 10^{12}$  Gauss and spin period of 30 ms, whereas for SG and OG models the phase-plots were computed for gap widths of 0.04 and 0.01, respectively. All plots have been obtained for a magnetic obliquity  $\alpha = 45$ . The emission intensity decreases from yellow to black. (Courtesy of Marco Pierbattista.)

In a nutshell, none of the models proposed so far is able to account for the phenomenology of the observed *Fermi*-LAT pulsars: OG and SG are generally better but not adequate to fit all objects. Some pulsars can be reasonably well fitted by more than one model, some by none.

## 5. PARADIGM LOST: WINNING THE PULSAR REVOLUTION

While the 2PC (Abdo et al. 2013) was being written, the gamma-ray pulsar family gained 15 more members that are listed in table 4 of the catalog. Of the new entries, 11 are MSPs while 4 are young radio pulsars. Since then, new detections have been announced, and as of June 2014, 147 NSs have been seen in gamma rays. Their parameters can be found at <https://confluence.slac.stanford.edu/display/GLAMCOG/Public+List+of+LAT-Detected+Gamma-Ray+Pulsars>. Thanks to the extremely successful synergy between radio and gamma-ray astronomy to find, characterize, and phase-fold MSPs, the number of MSP discoveries currently accounts for two-thirds of the new pulsars. However, one such MSP was not found through radio searches but rather through an original approach exploiting at once gamma-ray and optical astronomy. Performing blind searches for MSPs in binary systems is vastly more difficult than searching for young isolated pulsars, because the search must cover a much larger frequency interval, scanning for (at least three) additional unknown orbital parameters. This becomes an impossible task, even for the most powerful supercomputer. The source 0FGL J1311.9-3419, bright enough to be already listed in the very first *Fermi* Bright Source Catalog (Abdo et al. 2009g), however, yielded a valuable hint through its optical emission. In an observing campaign aimed at finding optical variation of MSPs' binary companions within unidentified *Fermi* sources, Romani (2012) detected a

quasi-sinusoidal 93-minute modulation that was thought to arise from a black-widow system (where the MSP irradiates its low-mass companion leading, eventually, to its evaporation). Indeed, the 93-m period is the shortest known for such a binary system. By focusing on the coordinates of the variable optical source and exploiting the tight constraints placed on the orbital parameters, Pletsch et al. (2012c) were able to detect a 2.5-ms MSP, the first found through a gamma-ray blind search, an historic accomplishment. However, PSR J1311-3430 is not the long-sought radio-quiet MSP: radio astronomers went back to the source, which had been already observed to no avail and, with considerable effort, Ray et al. (2013) found the radio signal that is present only during a small fraction of the radio observations. Further optical studies allowed Romani et al. (2012) to constrain the mass of the NS to be  $>2.1 M_{\odot}$ .

A similar optical strategy was applied to 0FGL J2339.8-0530. Variability pointed to a tentative orbital period (Romani & Shaw 2011) that was the driver behind a successful radio search that soon led to a gamma-ray detection listed in the 2PC (Abdo et al. 2013). Those success stories rest on new multiwavelength strategies that will certainly bring more results in the future.

### 5.1. 2013: Enter Citizen Science

Blind searches for gamma-ray pulsars are computationally intensive, thus any additional computer resource is most welcome. To increase (at no cost) the computer power to be used in their searches, Pletsch et al. (2013) exploited the potential of the volunteer distributed computer system Einstein@Home (E@H, Allen et al. 2013), a well-known Citizen Science project that was started in 2005 to search for GWs in data collected by the LIGO-Virgo Collaboration. By downloading the E@H software, volunteers agree to devote the power of their computer, when not in use, to perform the E@H tasks. With more than 300,000 volunteers, E@H is one of the most popular Citizen Science projects and averages a total computing power of 1 PFLOPS, comparable to the largest supercomputers. Since 2009, the system has been adapted to analyze radio telescope data, yielding several pulsar discoveries (Allen et al. 2013), and is now being used to perform blind searches on *Fermi* data. So far, four young pulsars have been discovered in unidentified 2FGL (Nolan et al. 2012) sources. Their parameters are characteristic of energetic objects relatively nearby, but none of them has yet been detected in radio. Considering the shortage of energetic radio-quiet pulsars, this result is remarkable. Two of the new pulsars have already been seen to glitch: PSR J1522-5734 glitched once, whereas PSR J1422-6138 glitched twice, proving that the system works well in spite of those timing jumps. The additional computer power provided by E@H combined with an improved search technique is a good omen for more findings, hopefully also of the long-sought radio-quiet MSP.

### 5.2. Breaking a Decade-Long Paradigm

The discovery of the Crab Nebula variability has been one of the most astonishing results in high-energy gamma-ray astronomy. On September 2010, a sudden enhancement of the overall Crab flux was reported first by AGILE and immediately confirmed by *Fermi* (Abdo et al. 2011, Tavani et al. 2011). A quick sequence of radio, X-ray, and optical observations made it clear that the pulsar was behaving normally. Indeed, in gamma rays the pulsed flux from the Crab was also unchanged, leaving the nebula as the only suspect for the flux increase. Moreover, the short timescale of the variability pointed to a quite small region of interest, possibly next to the pulsar. To achieve the highest angular resolution to study the interior of the Crab Nebula, near the pulsar, the *Chandra X-ray Observatory* and the *Hubble Space Telescope* (HST) were immediately triggered for target-of-opportunity (ToO) observations that were performed a few days after the

event. The high-resolution optical and X-ray images failed to show any dramatic change in the notoriously active Crab Nebula inner region. A search in both AGILE and *Fermi* data did prove that enhancements had been detected previously, making it clear that the Crab's September 2010 flaring episode was not a unique event but rather a recurring one. A massive ToO campaign was organized, waiting for the next flares, which were recorded in April 2011 (Striani et al. 2011, Buehler et al. 2012, Weisskopf et al. 2013) and March 2013 (Mayer et al. 2013), when both *Cbndra* and HST repeatedly observed the nebula. Once again, comparing images taken before, during, and after the flare, nothing obvious was seen to change. The Crab flares shine only in gamma rays, and such events are possibly linked to sudden particle acceleration (e.g., Buehler & Blandford 2014), driven perhaps by magnetic reconnection. Hopefully the coming years may provide more flares to test the various proposed theories.

In spite of the pulsar definition we have used so far, variability in INSs and in their surroundings may not be all that exceptional. Allafort et al. (2013) recently reported the detection of a significant flux variation; this time there was a decrease from PSR J2021+4026, a radio-quiet INS in the Cygnus region with an X-ray counterpart (Weisskopf et al. 2011). Judging from its light curve, PSR J2021+4026 is similar to Geminga and recently joined Geminga and CTA-1 in the very small club of radio-quiet gamma-ray pulsars seen to pulsate in X-rays (Lin et al. 2013). The gamma-ray flux decrease, which took place in less than a week, is associated with a 4% increase in the pulsar's spin-down rate and a change in the light curve. The timing parameters of the pulsar have changed in a way never before seen in gamma rays. A jump in  $P$  is typically followed by a recovery pattern. Moreover, flux variability has never been associated with a glitch, despite repeated analyses during major Vela glitches to search for such a behavior. Is the jump due to a shift in the magnetic field structure? If so, PSR J2021+4026 may have done it before, as AGILE has detected variability from this gamma-ray source (Chen et al. 2011), although the finding could not be linked to the pulsar. As puzzling as it may sound, these results may be heralding a new era where the pulsar steady flux paradigm is superseded.

## 6. NOW WHAT?

**Figure 13** provides a snapshot of the current census of *Fermi* pulsars (divided between radio-loud pulsars, radio-quiet pulsars, and MSPs) together with an overall view of four decades of pulsar studies in high-energy gamma rays. While the growth during the past five years is dramatic, to say the least, it is apparent that the most recent detections have changed the family balance, making MSPs the dominant class among the gamma-ray pulsar types. This is the unexpected, surprising, and really revolutionary result from the *Fermi* mission. Predicting the detection of more MSPs is easy on the basis of the discovery rate shown in **Figure 3**. The next pulsar catalog will be dominated by MSPs, many in black-widow systems.

Together with more MSPs, fainter young radio pulsars will be found (Hou et al. 2014) owing to a major *Fermi* software update, which promises improved sensitivity at low energies (Atwood et al. 2013). The statistical significance for faint sources builds up slowly, and endurance is required to spot the less energetic pulsars. However, this effort should be handsomely rewarded as the detections of even a handful of pulsars fainter than the current death line in the  $P - \dot{P}$  diagram will have important implications in pulsar physics. Moreover, lowering the  $\dot{E}$  threshold for gamma-ray detection would bring many more INS candidates into play, thus increasing their contribution to the overall Galactic emission while also providing an obvious source for the overabundance of positrons detected by the Pamela Collaboration (Adriani et al. 2009), *Fermi* (Ackerman et al. 2012b), and the AMS Collaboration (Aguilar et al. 2013).

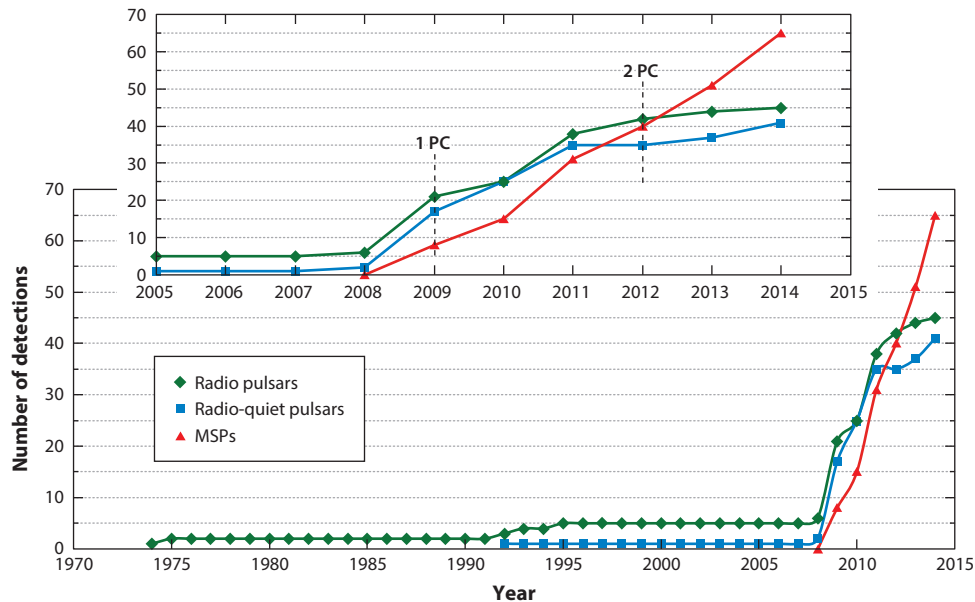


**Figure 13**

Pulsar census for radio-loud pulsars (*green diamonds*), radio-quiet pulsars (*blue squares*), and millisecond pulsars (MSPs, *red triangles*). The inset shows the dramatic advancements of the past five years. The pulsar accounting published in the first (1PC, Abdo et al. 2010b) and second (2PC, Abdo et al. 2013) pulsar catalogs are highlighted.

The discovery of gamma-quiet INs detected only at radio wavelengths is also an important goal because it would provide a missing piece of the puzzle for pulsar emission geometry. So far, all the INs we know of come in two flavors: radio-and-gamma and gamma-only. It is time to complete the picture with a few representatives of the gamma-quiet class. Detecting just unpulsed gamma-ray emission from a NS magnetosphere is also an intriguing possibility. But it will be hard to secure a convincing identification without a pulsar time signature.

By solving the riddle of dozens of previously unidentified gamma-ray sources, pulsars, be they young or recycled, prove to be the most promising candidates to account for a sizable fraction the remaining unassociated Galactic gamma-ray sources. By continuing to study unassociated sources, *Fermi* will certainly unveil many more surprising results.

Surprises may come also from the scores of INs already detected in gamma-rays. Although variability may be more common than previously thought, the combined use of many of the MSPs unveiled by *Fermi* may provide a tool to directly detect, at last, gravitational waves.

## DISCLOSURE STATEMENT

The author is not aware of any affiliations, memberships, funding, or financial holdings that might be perceived as affecting the objectivity of this review.

## ACKNOWLEDGMENTS

This paper is my own mostly first-hand account of the 40-year-long struggle to detect and understand gamma-ray emission from NSs. During this long time span, I enjoyed working and

discussing with many colleagues whose results and opinions I have tried to describe as accurately as possible.

I am indebted to the whole *Fermi* LAT collaboration, which did a tremendous job in changing our views of the gamma-ray sky. Working with the Galactic group has always been fun and stimulating. I have learned a lot from Alice Harding and Roger Romani, who have been the theoretical task force behind many *Fermi* papers and, quite rightly, have been awarded the 2013 Rossi prize for their contributions toward the understanding of gamma-ray pulsar emission. I am especially grateful to David Smith, who helped me to handle all the *Fermi*-related figures as well as the pulsar tables. I really appreciated his critical assessments and his clever suggestions. Elizabeth Ferrara and Pablo Saz Parkinson were kind enough to read and comment on the manuscript. To them my most sincere thanks for their time and their patience. Marco Pierbattista kindly provided **Figure 12**. I am also grateful to the Fermi Publication Board, which granted permission to use published material as well as unpublished data from the most recent pulsar census.

## LITERATURE CITED

- Abdo AA, Ackermann M, Ajello M, et al. (Fermi LAT Collab.) 2009a. *Astropart. Phys.* 32:193  
Abdo AA, Ackermann M, Ajello M, et al. (Fermi LAT Collab.) 2009b. *Ap. J. Lett.* 699:L102  
Abdo AA, Ackermann M, Ajello M, et al. (Fermi LAT Collab.) 2009c. *Science* 325:848  
Abdo AA, Ackermann M, Ajello M, et al. (Fermi LAT Collab.) 2009d. *Science* 325:845  
Abdo AA, Ackermann M, Ajello M, et al. (Fermi LAT Collab.) 2009e. *Science* 325:840  
Abdo AA, Ackermann M, Ajello M, et al. (Fermi LAT Collab.) 2009f. *Ap. J.* 700:1059  
Abdo AA, Ackermann M, Ajello M, et al. (Fermi LAT Collab.) 2009g. *Ap. J. Suppl.* 183:46  
Abdo AA, Ackermann M, Ajello M, et al. (Fermi LAT Collab.) 2010a. *Astron. Astrophys.* 524:75  
Abdo AA, Ackermann M, Ajello M, et al. (Fermi LAT Collab.) 2010b. *Ap. J. Suppl.* 187:460  
Abdo AA, Ackermann M, Ajello M, et al. (Fermi LAT Collab.) 2010c. *Ap. J.* 708:1254  
Abdo AA, Ackermann M, Ajello M, et al. (Fermi LAT Collab.) 2010d. *Ap. J.* 712:1209  
Abdo AA, Ackermann M, Ajello M, et al. (Fermi LAT Collab.) 2010e. *Ap. J.* 713:154  
Abdo AA, Ackermann M, Ajello M, et al. (Fermi LAT Collab.) 2010f. *Ap. J.* 720:272  
Abdo AA, Ackermann M, Ajello M, et al. (Fermi LAT Collab.) 2010g. *Ap. J. Suppl.* 188:405  
Abdo AA, Ackermann M, Ajello M, et al. (Fermi LAT Collab.) 2010h. *Ap. J.* 711:64  
Abdo AA, Ackermann M, Ajello M, et al. (Fermi LAT Collab.) 2011. *Science* 331:739  
Abdo AA, Ackermann M, Atwood WB, et al. (Fermi LAT Collab.) 2008. *Science* 322:1218  
Abdo AA, Ackermann M, Atwood WB, et al. (Fermi LAT Collab.) 2009h. *Ap. J. Lett.* 695:L72  
Abdo AA, Ackermann M, Atwood WB, et al. (Fermi LAT Collab.) 2009i. *Ap. J.* 696:1084  
Abdo AA, Ackermann M, Atwood WB, et al. (Fermi LAT Collab.) 2009j. *Ap. J.* 699:1171  
Abdo AA, Ajello M, Allafort A, et al. (Fermi LAT Collab.) 2013. *Ap. J. Suppl.* 208:17  
Ackermann M, Ajello M, Allafort A, et al. (Fermi LAT Collab.) 2012a. *Ap. J.* 753:83  
Ackermann M, Ajello M, Allafort A, et al. (Fermi LAT Collab.) 2012b. *Phys. Rev. Lett.* 108:011103  
Adriani O, Barbarino GC, Bazilevskaya GA (Pamela Collab.) 2009. *Nature* 448:607  
Aguilar M, Alberti G, Alpat B, et al. (AMS Collab.) 2013. *Phys. Rev. Lett.* 110:141102  
Aleksic J, Alvarez EA, Antonelli LA, et al. (MAGIC Collab.) 2012. *Astron. Astrophys.* 540:69  
Aliu E, Anderhub H, Antonelli LA, et al. (MAGIC Collab.) 2008. *Science* 322:1221  
Aliu E, Arlent T, Aune T, et al. (Veritas Collab.) 2011. *Science* 334:69  
Allafort A, Baldini L, Ballet J, et al. 2013. *Ap. J. Lett.* 777:L2  
Allen B, Knispel B, Cordes JM, et al. 2013. *Ap. J.* 773:91  
Arons J. 1983. *Ap. J.* 266:215  
Arons J. 1996. *Astron. Astrophys.* 129:49  
Atwood WB, Abdo AA, Ackermann M, et al. (Fermi LAT Collab.) 2009. *Ap. J.* 697:1071  
Atwood WB, Baldini L, Bregeon J, et al. 2013. *Ap. J.* 774:76  
Atwood WB, Ziegler M, Johnson RP, Baughman BM. 2006. *Ap. J. Lett.* 652:L49

- Bai XN, Spitkovsky A. 2010. *Ap. J.* 715:1282
- Baldini L, Bastieri L, Boinee D, et al. 2006. *Nuclear Phys. B Proc. Suppl.* 150:62
- Baring M. 2004. *Adv. Space Res.* 33:552
- Bennett K, Bignami GF, Boella G, et al. 1977. *Astron. Astrophys.* 61:279
- Bertsch DL, Brazier KTS, Fichtel CE, et al. 1992. *Nature* 357:306
- Bignami GF. 2008. *Science* 322:1193
- Bignami GF, Bennett K, Buccheri R, et al. 1981a. *Astron. Astrophys.* 93:71
- Bignami GF, Boella G, Burger JJ, et al. 1975. *Space Sci. Instrum.* 1:245
- Bignami GF, Caraveo PA. 1980. *Ap. J.* 241:1161
- Bignami GF, Caraveo PA. 1992. *Nature* 357:287
- Bignami GF, Caraveo PA. 1996. *Ann. Rev. Astron. Astrophys.* 34:331
- Bignami GF, Caraveo PA, Lamb RC. 1983. *Ap. J. Lett.* 272:L9
- Bignami GF, Caraveo PA, Lamb RC, Markert TH, Paul JA. 1981b. *Ap. J. Lett.* 247:L85
- Bignami GF, Hermsen W. 1983. *Annu. Rev. Astron. Astrophys.* 21:67
- Brazier KTS, Kanbach G, Carramiñana A, Guichard J, Merck M. 1996. *MNRAS* 281:1033
- Brazier KTS, Reimer O, Kanbach G, Carramiñana A. 1998. *MNRAS* 295:819
- Buccheri R, Bennett K, Bignami GF, et al. 1983. *Astron. Astrophys.* 128:245
- Buccheri R, D'Amico N, Massaro E, Scarsi L. 1978. *Nature* 274:572
- Buehler R, Scargle JD, Blandford RD, et al. 2012. *Ap. J.* 749:26
- Bühler R, Blandford R. 2014. *Rep. Prog. Phys.* 77:066901
- Bulgarelli A, Tavani M, Caraveo P, et al. 2008. *Astron. Astrophys.* 489:L17
- Camilo F, Kerr M, Ray PS, et al. 2012. *Ap. J.* 746:39
- Camilo F, Ray PS, Ransom SM, et al. 2009. *Ap. J.* 705:1
- Caraveo PA. 1982. *Space Sci. Rev.* 36:207
- Caraveo PA. 2010. *Proc. HTRA-IV Agios Nikolaos, Crete, Greece, May 5–7*. arXiv:10092421
- Caraveo PA, Bignami GF, De Luca A, et al. 2003. *Science* 301:1345
- Caraveo PA, De Luca A, Marelli M, et al. 2010. *Ap. J. Lett.* 725:L6
- Caraveo PA, De Luca A, Mereghetti S, Pellizzoni A, Bignami GF. 2004. *Science* 305:376
- Chen AW, Piano G, Tavani M, et al. 2011. *Astron. Astrophys.* 525:33
- Cheng KS, Ho C, Ruderman M. 1986. *Ap. J.* 300:500
- Chiang J, Romani RW. 1992. *Ap. J.* 400:692
- Chiang J, Romani RW. 1994. *Ap. J.* 436:754
- Cognard I, Guillemot L, Johnson TJ, et al. 2011. *Ap. J.* 732:47
- Cordes JM, Shannon RM. 2012. *Ap. J.* 750:89
- Coroniti FV. 1990. *Ap. J.* 349:538
- D'Amico N, Kaspi VM, Manchester RN, et al. 2001. *Ap. J. Lett.* 552:L45
- Daugherty JK, Harding AK. 1982. *Ap. J.* 252:337
- Daugherty JK, Harding AK. 1996. *Ap. J.* 458:278
- de Jager OC, Büsching I. 2010. *Astron. Astrophys.* 517:L9
- de Jager OC, Raubenheimer BC, Swanepoel JWH. 1989. *Astron. Astrophys.* 221:180
- De Luca A, Caraveo PA, Mattana F, Pellizzoni A, Bignami GF. 2006. *Astron. Astrophys.* 445:L9
- De Luca A, Caraveo PA, Mereghetti S, Negroni M, Bignami GF. 2005. *Ap. J.* 623:1051
- Dormody M, Johnson RP, Atwood WB. 2011. *Ap. J.* 742:126
- Dyks J, Rudak B. 2003. *Ap. J.* 598:1201
- Fichtel CE, Hartman RC, Kniffen DA, et al. 1975. *Ap. J.* 198:163
- Fierro JM, Bertsch DL, Brazier, et al. 1993. *Ap. J. Lett.* 413:L27
- Freire PCC, Abdo AA, Ajello M, et al. 2011. *Science* 334:1107
- Gehrels N, Chipman E, Kniffen D. 1994. *Ap. J. Suppl.* 92:351
- Gehrels N, Macomb DJ, Bertsch DL, Thompson DJ, Hartman RC. 2000. *Nature* 40:363
- Goldreich P, Julian WH. 1969. *Ap. J.* 157:869
- Grenier I, Hermsen W, Clear J. 1988. *Astron. Astrophys.* 204:117
- Guillemot L, Tauris TM. 2014. *MNRAS* 439:2033–42
- Halpern JP, Camilo F, Giuliani A, et al. 2008. *Ap. J. Lett.* 688:L33

- Halpern JP, Camilo F, Gotthelf EV, et al. 2001a. *Ap. J. Lett.* 552:L125
- Halpern JP, Gotthelf EV, Camilo F, Helfand DJ, Ransom SM. 2004. *Ap. J.* 612:398
- Halpern JP, Gotthelf EV, Leighly KM, Helfand DJ. 2001b. *Ap. J.* 547:323
- Halpern JP, Gotthelf EV, Mirabal N, Camilo F. 2002. *Ap. J. Lett.* 573:L41
- Halpern JP, Holt SS. 1992. *Nature* 357:222
- Harding AK, Gonthier PL, Ouellette MS, O'Brien S, Berrier J. 2002. In *Neutron Stars in Supernova Remnants*, ed. PO Slane, BM Gaensler. *ASP Conf. Ser.* 271:335. San Francisco: ASP.
- Harding AK, Grenier I, Gonthier PL. 2007. *Astrophys. Space Sci.* 309:221
- Harding AK, Tadamaru E, Esposito LW. 1978. *Ap. J.* 225:226
- Harding AK, Usov V, Muslimov V, Alex G. 2005. *Ap. J.* 622:531
- Hartman RC, Bertsch DL, Bloom SD, et al. 1999. *Ap. J. Suppl.* 123:79
- Hirokami K, Harding AK, Shibata S. 2003. *Ap. J.* 591:334
- Hou X, Smith D, Reposeur T, Rousseau R. 2014. *Astron. Nachr.* 335(3):334
- Jackson MS, Halpern JP. 2005. *Ap. J.* 633:1114
- Jenet FA, Hobbs GB, Lee KJ, Manchester RN. 2005. *Ap. J. Lett.* 625:L123
- Kanbach G, Arzoumanian Z, Bertsch DL, et al. 1994. *Astron. Astrophys.* 289:855
- Kanbach G, Bennett K, Bignami GF, et al. 1980. *Astron. Astrophys.* 90:163
- Kanbach G, Bertsch DL, Fichtel CE, et al. 1988. *Space Sci. Rev.* 49:69
- Kaspi VM, Lackey JR, Mattox J, et al. 2000. *Ap. J.* 528:445
- Keith MJ, Johnston S, Kramer M, et al. 2008. *MNRAS* 389:1881
- Keith MJ, Johnston S, Ray PS, et al. 2011. *MNRAS* 414:1292
- Kerr M. 2011. *Ap. J.* 732:38
- Kerr M, Camilo F, Johnson TJ, et al. 2012. *Ap. J. Lett.* 748:L2
- Kong AKH, Hui CY, Cheng KS. 2010. *Ap. J. Lett.* 712:L36
- Kniffen DA, Hartman RC, Thompson DJ, Bignami GF, Fichtel CE. 1974. *Nature* 251:397
- Kramer M, Bell JF, Manchester RN, et al. 2003. *MNRAS* 342:1299
- Kuiper L, Hermsen W, Cusumano G, et al. 2001. *Astron. Astrophys.* 378:918–35
- Kuiper L, Hermsen W, Krijger JM, et al. 1999. *Astron. Astrophys.* 351:119
- Kuiper L, Hermsen W, Verbunt F, et al. 2000. *Astron. Astrophys.* 359:615
- Lin LCC, Hui CY, Hu CP, et al. 2013. *Ap. J. Lett.* 770:L9
- Marelli M. 2012. *The X-Ray Behaviour of Fermi/LAT Pulsars*. PhD thesis, Univ. Insubria, Como, Italy. arXiv:1205.1748
- Marelli M, De Luca A, Caraveo PA. 2011. *Ap. J.* 733:82
- Mattox JR, Bertsch DL, Fichtel CE, et al. 1992. *Ap. J. Lett.* 401:L23
- Mayer M, Buehler R, Hays E, et al. 2013. *Ap. J. Lett.* 775:L37
- Mayer-Hasselwander HA, Bertsch DL, Brazier KTS, et al. 1994. *Ap. J.* 421:276
- Meehan C, Lichti G, Bhat PN, et al. (GBM Collab.) 2009. *Ap. J.* 702:791
- Mirabal N, Halpern JP. 2001. *Ap. J. Lett.* 547:L137
- Mukherjee R, Bertsch DL, Dingus BL. 1995. *Ap. J. Lett.* 441:L61
- Muslimov AG, Harding AK. 2003. *Ap. J.* 588:430
- Muslimov AG, Harding AK. 2004. *Ap. J.* 606:1143
- Nel HI, Arzoumanian Z, Bailes M, et al. 1996. *Ap. J.* 465:898
- Ng C-Y, Roberts MSE, Romani RW. 2005. *Ap. J.* 627:904
- Nolan PL, Abdo AA, Ackermann M, et al. (Fermi LAT Collab.) 2012. *Ap. J. Suppl.* 199:31
- Nolan PL, Arzoumanian Z, Bertsch DL, et al. 1993. *Ap. J.* 409:697
- Ogelman H, Fichtel CE, Kniffen DA, Thompson DJ. 1976. *Ap. J.* 209:584
- Pavlov GG, Bhattacharyya S, Zavlin VE. 2010. *Ap. J.* 715:66
- Pellizzoni A, Pilia M, Possenti A, et al. 2009a. *Ap. J.* 691:1618
- Pellizzoni A, Pilia M, Possenti A, et al. 2009b. *Ap. J. Lett.* 695:L115
- Pellizzoni A, Trois A, Tavani M, et al. 2010. *Science* 327:663
- Petri J. 2011. *MNRAS* 412:1870
- Pierbattista M. 2010. PhD thesis, Université Paris 7, Denis Diderot. arXiv:1309.5982
- Pierbattista M, Grenier IA, Harding AK, Gonthier PL. 2012. *Astron. Astrophys.* 545A:42P

- Pilia M, Pellizzoni A, Trois A, et al. 2010. *Ap. J.* 723:707
- Pineault S, Landecker TL, Mardore B, Gaumont-Guay S. 1993. *Astron. J.* 105:1060
- Pletsch HJ, Guillemot L, Allen B, et al. 2012a. *Ap. J.* 744:105
- Pletsch HJ, Guillemot L, Allen B, et al. 2012b. *Ap. J. Lett.* 755:L20
- Pletsch HJ, Guillemot L, Allen B, et al. 2013. *Ap. J. Lett.* 779:L11
- Pletsch HJ, Guillemot L, Fehrmann HA, et al. 2012c. (Fermi LAT Collab.) *Science* 338:1314
- Ramanamurthy PV, Bertsch DL, Dingus BL, et al. 1995. *Ap. J. Lett.* 447:L109
- Ramanamurthy PV, Fichtel CE, Harding AK, et al. 1996. *Astron. Astrophys. Suppl.* 120:115
- Ransom SM, Ray PS, Camilo F, et al. 2011. *Ap. J. Lett.* 727:L16
- Ravi V, Manchester RN, Hobbs G. 2010. *Ap. J. Lett.* 716:L85
- Ray PS, Abdo AA, Parent D, et al. 2012. *Proc. 2011 Fermi Symp., Rome, Italy, May 9–12*, eConf C110509. arXiv:12053089
- Ray PS, Kerr M, Parent D, et al. 2011. *Ap. J. Suppl.* 194:17
- Ray PS, Ransom SM, Cheung CC, et al. 2013. *Ap. J. Lett.* 763:L13
- Razzano M, Harding AK, Baldini L, et al. 2009. *Astropart. Phys.* 32:1
- Reimer O, Brazier KTS, Carramiñana A, et al. 2001. *MNRAS* 324:772
- Roberts MSE. 2013. In *Neutron Stars and Pulsars: Challenges and Opportunities after 80 Years, Proc. IAU Symp. 291*, ed. J van Leeuwen, 8:127–32. Cambridge, UK: Cambridge Univ. Press
- Roberts MSE, Brogan CL. 2008. *Ap. J.* 681:320
- Roberts MSE, Hessels JWT, Ransom SM, et al. 2002. *Ap. J. Lett.* 577:L19
- Roberts MSE, Romani RW, Kawai N. 2001. *Astron. Astrophys. Suppl.* 133:451
- Romani RW. 1996. *Ap. J.* 470:469
- Romani RW. 2012. *Ap. J. Lett.* 754:L25
- Romani RW, Filippenko AV, Silverman JM, et al. 2012. *Ap. J. Lett.* 760:L36
- Romani RW, Kerr M, Craig HA, et al. 2011. *Ap. J.* 738:114
- Romani RW, Shaw MS. 2011. *Ap. J. Lett.* 743:L26
- Romani RW, Watters KP. 2010. *Ap. J.* 714:810
- Romani RW, Yadigaroglu IA. 1995. *Ap. J.* 438:314
- Ruderman MA, Sutherland PG. 1975. *Ap. J.* 196:51
- Saz Parkinson PM, Belfiore A, Dormody M, et al. (Fermi LAT Collab.) 2012. *Proc. 2011 Fermi Symp. Rome, Italy, May 9–12*.
- Saz Parkinson PM, Dormody M, Ziegler M, et al. 2010. *Ap. J.* 725:571
- Saz Parkinson PM (Fermi LAT Collab.). 2009. In *Science with the New Generation of High Energy Gamma-Ray Experiments : Bridging the Gap Between GeV and TeV*. AIP Conf. Proc., 1112:79
- Smith DA, Guillemot L, Camilo F, et al. 2008. *Astron. Astrophys.* 492:923
- Smith DA, Thompson DJ. 2009. In *Neutron Stars Pulsars*, ed. W Becker. *Astrophys. Space Sci. Libr.* 357:621. Heidelberg, Ger.: Springer-Verlag
- Striani E, Tavani M, Piano G, et al. 2011. *Ap. J. Lett.* 741:L5
- Sturrock PA. 1971. *Ap. J.* 164:529
- Swanenburg BN, Bennett K, Bignami GF, et al. 1981. *Ap. J. Lett.* 243:L69
- Tavani M, Barbiellini G, Argan A, et al. (Agile Collab.) 2009. *Astron. Astrophys.* 502:995
- Tavani M, Bulgarelli A, Vittorini V, et al. 2011. *Science* 331:736
- Thompson DJ. 2001. In *Int. Symp. High-Energy Gamma-Ray Astron. Heidelberg, Ger.*, FA Aharonian, HJ Völk. *AIP Conf. Proc.* 558:103–14. Melville, NY: AIP
- Thompson DJ. 2004. In *Cosmic Gamma-Ray Sources*, ed. KS Cheng, GE Romero. *Astrophys. Space Sci. Libr.* 304:149. Dordrecht, Neth.: Springer
- Thompson DJ, Arzoumanian Z, Bertsch DL, et al. 1992. *Nature* 359:615
- Thompson DJ, Bailes M, Bertsch DL, et al. 1996. *Ap. J.* 465:385
- Thompson DJ, Bailes M, Bertsch DL, et al. 1999. *Ap. J.* 516:297
- Thompson DJ, Fichtel CE, Kniffen DA, Ogelman HB. 1975. *Ap. J. Lett.* 200:L79
- Vasseur JP, Parlier J, Leray B, et al. 1971. *Nature* 233:46
- Vasseur JP, Parlier J, Leray B, Forichon JP, Agrinier M. 1970. *Nature* 226:534

- Venter C, Harding AK, Guillemot L. 2009. *Ap. J.* 707:800
- Venter C, Johnson TJ, Harding AK. 2012. *Ap. J.* 744:34
- Watters KP, Romani RW. 2011. *Ap. J.* 727:123
- Watters KP, Romani RW, Weltevrede P, Johnston S. 2009. *Ap. J.* 695:1289
- Weisskopf MC, Romani RW, Razzano M, et al. 2011. *Ap. J.* 743:74
- Weisskopf MC, Tennant AF, Arons J, et al. 2013. *Ap. J.* 765:56
- Yadigaroglu I-A, Romani RW. 1995. *Ap. J.* 449:211
- Ziegler M, Baughman BM, Johnson RP, Atwood WB. 2008. *Ap. J.* 680:620



# Contents

Wondering About Things <i>George B. Field</i> .....	1
Short-Duration Gamma-Ray Bursts <i>Edo Berger</i> .....	43
Observational Clues to the Progenitors of Type Ia Supernovae <i>Dan Maoz, Filippo Mannucci, and Gijs Nelemans</i> .....	107
Tidal Dissipation in Stars and Giant Planets <i>Gordon I. Ogilvie</i> .....	171
Gamma-Ray Pulsar Revolution <i>Patrizia A. Caraveo</i> .....	211
Solar Dynamo Theory <i>Paul Charbonneau</i> .....	251
The Evolution of Galaxy Structure Over Cosmic Time <i>Christopher J. Conselice</i> .....	291
Microarcsecond Radio Astrometry <i>M. J. Reid and M. Honma</i> .....	339
Far-Infrared Surveys of Galaxy Evolution <i>Dieter Lutz</i> .....	373
Cosmic Star-Formation History <i>Piero Madau and Mark Dickinson</i> .....	415
Mass Loss: Its Effect on the Evolution and Fate of High-Mass Stars <i>Nathan Smith</i> .....	487
Hot Accretion Flows Around Black Holes <i>Feng Yuan and Ramesh Narayan</i> .....	529
The Coevolution of Galaxies and Supermassive Black Holes: Insights from Surveys of the Contemporary Universe <i>Timothy M. Heckman and Philip N. Best</i> .....	589

Numerical Relativity and Astrophysics <i>Luis Lehner and Frans Pretorius</i> .....	661
---	-----

## **Indexes**

Cumulative Index of Contributing Authors, Volumes 41–52 .....	695
Cumulative Index of Article Titles, Volumes 41–52 .....	698

## **Errata**

An online log of corrections to *Annual Review of Astronomy and Astrophysics* articles may be found at <http://www.annualreviews.org/errata/astro>



# ANNUAL REVIEWS

It's about time. Your time. It's time well spent.

## New From Annual Reviews:

### ***Annual Review of Statistics and Its Application***

Volume 1 • Online January 2014 • <http://statistics.annualreviews.org>

Editor: **Stephen E. Fienberg**, *Carnegie Mellon University*

Associate Editors: **Nancy Reid**, *University of Toronto*

**Stephen M. Stigler**, *University of Chicago*

The *Annual Review of Statistics and Its Application* aims to inform statisticians and quantitative methodologists, as well as all scientists and users of statistics about major methodological advances and the computational tools that allow for their implementation. It will include developments in the field of statistics, including theoretical statistical underpinnings of new methodology, as well as developments in specific application domains such as biostatistics and bioinformatics, economics, machine learning, psychology, sociology, and aspects of the physical sciences.

**Complimentary online access to the first volume will be available until January 2015.**

#### TABLE OF CONTENTS:

- *What Is Statistics?* Stephen E. Fienberg
- *A Systematic Statistical Approach to Evaluating Evidence from Observational Studies*, David Madigan, Paul E. Stang, Jesse A. Berlin, Martijn Schuemie, J. Marc Overhage, Marc A. Suchard, Bill Dumouchel, Abraham G. Hartzema, Patrick B. Ryan
- *The Role of Statistics in the Discovery of a Higgs Boson*, David A. van Dyk
- *Brain Imaging Analysis*, F. DuBois Bowman
- *Statistics and Climate*, Peter Guttorp
- *Climate Simulators and Climate Projections*, Jonathan Rougier, Michael Goldstein
- *Probabilistic Forecasting*, Tilmann Gneiting, Matthias Katzfuss
- *Bayesian Computational Tools*, Christian P. Robert
- *Bayesian Computation Via Markov Chain Monte Carlo*, Radu V. Craiu, Jeffrey S. Rosenthal
- *Build, Compute, Critique, Repeat: Data Analysis with Latent Variable Models*, David M. Blei
- *Structured Regularizers for High-Dimensional Problems: Statistical and Computational Issues*, Martin J. Wainwright
- *High-Dimensional Statistics with a View Toward Applications in Biology*, Peter Bühlmann, Markus Kalisch, Lukas Meier
- *Next-Generation Statistical Genetics: Modeling, Penalization, and Optimization in High-Dimensional Data*, Kenneth Lange, Jeanette C. Papp, Janet S. Sinsheimer, Eric M. Sobel
- *Breaking Bad: Two Decades of Life-Course Data Analysis in Criminology, Developmental Psychology, and Beyond*, Elena A. Erosheva, Ross L. Matsueda, Donatello Telesca
- *Event History Analysis*, Niels Keiding
- *Statistical Evaluation of Forensic DNA Profile Evidence*, Christopher D. Steele, David J. Balding
- *Using League Table Rankings in Public Policy Formation: Statistical Issues*, Harvey Goldstein
- *Statistical Ecology*, Ruth King
- *Estimating the Number of Species in Microbial Diversity Studies*, John Bunge, Amy Willis, Fiona Walsh
- *Dynamic Treatment Regimes*, Bibhas Chakraborty, Susan A. Murphy
- *Statistics and Related Topics in Single-Molecule Biophysics*, Hong Qian, S.C. Kou
- *Statistics and Quantitative Risk Management for Banking and Insurance*, Paul Embrechts, Marius Hofert

Access this and all other Annual Reviews journals via your institution at [www.annualreviews.org](http://www.annualreviews.org).

**ANNUAL REVIEWS | Connect With Our Experts**

Tel: 800.523.8635 (US/CAN) | Tel: 650.493.4400 | Fax: 650.424.0910 | Email: [service@annualreviews.org](mailto:service@annualreviews.org)

